A study on the internal quantum efficiency and light extraction efficiency of ultraviolet-emitting AlGaN nanowire structures by molecular beam epitaxy

Jiaying Lu

Department of Electrical and Computer Engineering
McGill University, Montreal, Quebec, Canada

A thesis submitted to McGill University in partial fulfillment of the requirement of the degree of Master of Science in Electrical Engineering

Abstract

Aluminum gallium nitride (AlGaN), with a wide and tunable energy gap, has been recognized as an ideal candidate for semiconductor ultraviolet (UV) light sources, including light-emitting diodes (LEDs) and lasers, for promising applications to water/air purification, sensing, just to name a few. Particularly, in the form of nanowires, the large surface-to-bulk volume ratio can accommodate lattice strain and promote dopant incorporation. Nonetheless, the efficiency of AlGaN nanowire UV LEDs remains extremely low. In general, the overall efficiency is associated with light extraction efficiency (LEE) and internal quantum efficiency (IQE). A better understanding of these efficiencies is thus necessary to further improve the overall device performance and efficiency. In this thesis, we first investigate the optical properties of AlGaN nanowires grown by molecular beam epitaxy (MBE), which is a catalyst-free, extremely pure, and atomic-precise growth technique. Through a theoretical model combining the excitation dependent photoluminescence (PL), the Al content dependent IQE for Al content in the range of 22 - 54 mol% is derived. Moreover, the effectiveness of a thin aluminum nitride (AlN) buffer layer on improving the AlGaN nanowire optical quality is further unveiled. In this thesis, we have also investigated the LEE of AlGaN nanowire photonic crystal UV LEDs emitting at 225 nm using 3D finite-difference time-domain (FDTD) method. The effects of various photonic crystal structures, as well as nanowire radii and spacings on LEE are examined. Moreover, the photonic band structures are calculated in order to understand the mechanisms for the LEE enhancement compared to conventional planar devices.

Abrégé

Nitrure d'aluminium-gallium (AlGaN), avec un écart d'énergie large et réglable, a été considéré comme un candidat idéal pour les sources de lumière ultraviolette (UV) à semi-conducteurs, y compris les diodes électroluminescentes (LED) et les lasers, pour des applications prometteuses pour la purification de l'eau ou l'air, la détection, pour n'en nommer que quelques-unes. En particulier, sous la forme de nanofils, le grand rapport surface / volume en vrac peut s'adapter à la déformation du réseau et favoriser l'incorporation de dopant. Pourtant, l'efficacité extrêmement faible des LED UV à nanofils AlGaN est associée à l'efficacité d'extraction de la lumière (LEE), et à l'efficacité quantique interne (IQE). Une estimation précise de ces paramètres conduit à une meilleure compréhension des problèmes potentiels de l'appareil et donc à une amélioration supplémentaire des performances. Dans ce mémoire de maîtrise, la caractérisation optique de nanofils AlGaN cultivés dans différentes conditions est réalisée par l'épitaxie par jet moléculaire, qui est une technique de croissance sans catalyseur, extrêmement pure et atomique précise. Grâce à un modèle théorique combinant la photoluminescence (PL) dépendante de l'excitation, l'IQE dépendant de la teneur en Al pour une teneur en Al dans la plage de 22 à 54 % en mole est déterminée. De plus, l'efficacité d'une fine couche tampon nitrure d'aluminium (AlN) sur l'amélioration de la qualité optique des nanofils d'AlGaN est confirmée. Dans ce travail, nous avons estimé aussi le LEE de LED UV à cristaux photoniques à nanofils AlGaN émettant à 225 nm en utilisant la méthode du domaine de temps à différence finie (FDTD) 3D. Les effets de cristaux photoniques différents, rayons de nanofils et espacements sur LEE sont examinés avec le calcul de la structure de la bande de cristal photonique pour comprendre les mécanismes de l'amélioration du LEE en comparaison aux disponsitifs planaires conventionnels.

Preface and author contribution

This manuscript-based thesis evaluates the internal quantum efficiency of AlGaN nanowires grown by molecular beam epitaxy as well as the light extraction efficiency of AlGaN nanowire photonic crystal structures on Si for their applications to UV LEDs. These studies aim to improve the overall efficiency of AlGaN nanowire deep UV LEDs.

Chapters 1 and 2 give a brief overview of AlGaN nanowires and a summary of the literature review. Chapter 3 to Chapter 5 present three manuscripts, with two published in *Journal of Vacuum Science & Technology B*, one published in *Journal of Nanophotonics*. The manuscripts published in *Journal of Vacuum Science & Technology B* are experimental work. The samples for these two manuscripts were prepared by Yun Zhong. The manuscript published in *Journal of Nanophotonics* is theoretical work, and the simulation was carried out by Jiaying Lu, with help from Mohammad Fazel Vafadar. Chapters 6 summarizes the research results and discusses future research opportunities.

Acknowlegement

It is my great pleasure to have Prof. Songrui Zhao being my supervisor and guiding me. He is always there for his students to provide help when they encounter any difficulties in the research work and keeps track of their research progress. Although 2020-2021 has been a tough year for all the members at McGill University, Prof. Zhao has joined our group members together through regular meetings and is able to provide timely feedback to our results. It is his continuous support, motivation, and guidance that make me complete my research work and this thesis.

I would also like to acknowledge my peers in Prof. Zhao's group for their support. Their accompany has made my life at McGill full of joys and has assisted me in my research work. I am especially thankful to Yun Zhong for growing the AlGaN nanowire samples by molecular beam epitaxy, and to Mohammad Fazel Vafadar for helping on the computation of photonic crystal band structures of different lattices.

I am grateful for all the faculty members and administrative staff at the Department of Electrical and Computer Engineering who have offered a pleasurable atmosphere for my graduate study at McGill University. I am also grateful for the staff at the Facility for Electron Microscopy Research at McGill University. I would like to express my great appreciation to Dr. David Liu for his help on taking transmission electron microscope images and training on scanning electron microscope. I would also like to thank Dr. Zhao Lu from McGill Nanotools-Microfab for providing the cleanroom wet bench training and HF training for me.

Last but not the least, I am extremely grateful for my parents who have provided unconditional support towards my study without whom I would not be able to have today's achievements.

Table of content

Caption List

List of Acronyms

AlGaN	Aluminum Gallium Nitride
AlN	Aluminum Nitride
CVD	Chemical Vapor Deposition
EQE	External Quantum Efficiency
FC	Flip-Chip
FDTD	Finite-Difference Time-Domain
FF	Fill Factor
GaCl	Galium Chloride
GaN	Gallium Nitride
H_2	Hydrogen
HVPE	Hydride Vapor Phase Epitaxy
ICP	Inductively Coupled Plasma
IE	Injection Efficiency
InGaN	Indium Gallium Nitride
IQE	Internal Quantum Efficiency
LED	Light-Emitting Diodes
LEE	Light Extraction Efficiency
LITG	Light-Induced Transient Grating
MBE	Molecular Beam Epitaxy
MOCVD	Metalorganic Chemical Vapor Deposition
MQW	Multiple Quantum Well
N_2	Nitrogen
NH_3	Ammonia

PhC	Photonic Crystal
PL	Photoluminescence
PSS	Patterned Sapphire Substrate
QCSE	Quantum Confined Stark Effect
RF	Radio Frequency
RHEED	Reflection High Energy Electron Diffraction
SAG	Selective Area Growth
SCCM	Standard Cubic Centimeters Per Minute
SEM	Scanning Electron Microscope
SiO_2	Silicon Dioxide
Si_xN_y	Silicon Nitride
SRH	Shockley-Read Hall
TDD	Threading Dislocation Density
TE	Transverse Electric
TEGa	Triethylgallium
TEM	Transmission Electron Microscope
TiO_2	Titanium Dioxide
TIR	Total Internal Reflection
TM	Transverse Magnetic
TMGa	Trimethylgallium
TRPL	time-resolved photoluminescence
UV	Ultraviolet
VLS	Vapor-Liquid-Solid
WPE	Wall-plug Efficiency

1. Introduction

1.1. Motivations

Deep ultraviolet (UV) light-emitting devices have a great number of applications, ranging from water/air purification, medical sensing, to sterilization. In this context, aluminum gallium nitride (AlGaN), owing to its wide and tunable energy bandgap energies (~3.4-6.1 eV), has received wide attention in the past decades for its promising future in fabricating semiconductor UV light-emitting diodes (LEDs). Compared with traditional UV light sources (e.g., mercury lamps), AlGaN UV LEDs provide several advantages such as environment-friendly, nontoxic, no requirement of warm-up time, and a much longer lifetime.[1]

The history of developing AlGaN UV LEDs can be traced back to 1990s.[2-4] However, even today, it has remained challenging to obtain high-efficiency AlGaN deep UV LEDs. One major obstacle is the high threading dislocation densities (TDDs), mainly due to the large lattice mismatch between the semiconductor layers and foreign substrates. In this regard, different technologies have been developed to reduce TDDs, including buffer layers, epitaxial lateral overgrowth, and superlattices.[5-7] Nonetheless, the TDDs have remained high (10^8 – 10^9 cm^{-2}) for the layers grown on sapphire (the most common foreign substrate). In recent years, although the use of bulk aluminum nitride (AlN) substrates can reduce TDDs drastically, the cost of bulk AlN substrates is extremely high, and only a small wafer size is available.

P-type doping into AlGaN is another critical issue for realizing electrically injected devices, due to the large Mg activation energy and compensation effects.[8] Moreover, at elevated growth temperature, the high Mg dopant surface desorption rate further aggravates this problem.[9] In the past, extensive efforts have been made to address this issue, such as polarization-induced doping by compositional grading in AlGaN.[10]

Other major challenges include poor light extraction efficiency and large electric polarization fields.[4, 11-13]

A different route to solve these challenges may be using nanowire structures. AlGaN in the form of one-dimensional and/or quasi-one-dimensional structures, such as nanowires, have natural advantages compared with their thin film counterparts and have emerged as an attractive platform for UV light-emitting devices. The large surface-to-bulk volume ratio of nanowires provides efficient lattice strain relaxation. The reduced strain also minimizes the piezoelectric field in nanowire structures and thus mitigates the quantum-confined Stark effect (QCSE), which is often observed in planar quantum wells.[5] More importantly, it has also been shown that in nanowire structures, the dopant incorporation can be enhanced drastically, benefitted from the enhanced surface doping.[14, 15] For example, free hole concentrations up to ~6×10^{17} cm^{-3} have been reported in AlN nanowires by virtue of the much enhanced Mg-dopant incorporation in AlN nanowires than that in AlN epilayers.[16]

The form of nanowires also allows more freedom in wafer selection other than Si substrate. Zhao et al. fabricated indium gallium nitride (InGaN)/GaN LEDs on Ti coated bulk polycrystalline Mo substrate.[17] Sarwar et al. reported the growth of GaN nanowires on Ti and Mo films with a similar optical quality compared to those grown on Si despite the delamination of the metal layers from Si substrate.[18] The growth of nanowires on flexible substrates is also possible, paving the way to roll-to-roll manufacturing. Prof. Myers' group reported the molecular beam epitaxy (MBE) growth of GaN nanowires LEDs on Ta and Ti foils with a turn-on voltage of ~5 V.[19]

1.2. Performance of AlGaN nanowire UV LED

The performance of AlGaN nanowire UV LEDs can be characterized by wall-plug

efficiency (WPE), which is a typical parameter to characterize LEDs. WPE is defined as the ratio of the output optical power to the input electrical power. It is a simple measure of how efficient a LED device can convert electricity to light; nonetheless, it only reveals limited information about the potential issues that limit the device performance.[20] In this context, another parameter, external quantum efficiency (EQE), decomposed from WPE, is often used for the device performance limitation analysis. **Figure 1** shows the EQE versus the emission wavelength for III-nitride nanowire LEDs in UV-blue spectrum. A general trend is the reduction of EQE as the wavelength reduces to UV range, which marks the transition from InGaN material system to AlGaN material system. Accompanied with the decreasing EQE is the extremely low optical output power, associated with inefficient current conduction and heat dissipation.[21]

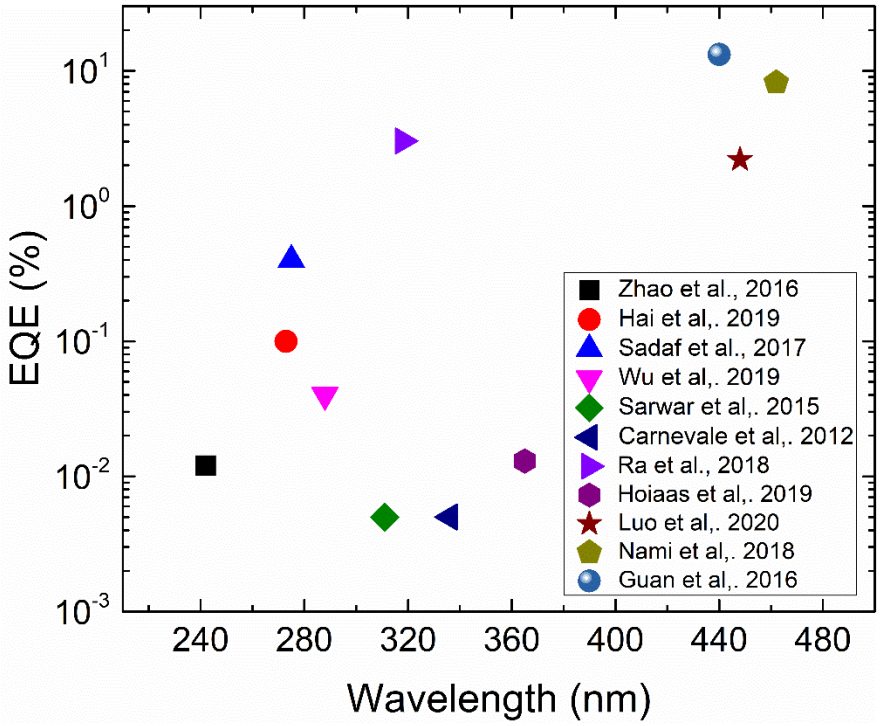

Fig. 1 EQE of III-nitride nanowire LEDs with emission wavelength spanning from blue to UV range from the literature. Data points are obtained from Refs. [21-31].

In order to better understand the causes of the drop of efficiency as the wavelength reduces, the EQE can be further decomposed into several descendent factors according to Eq. 1, namely, internal quantum efficiency (IQE), carrier injection efficiency (IE), and light extraction efficiency (LEE). To improve EQE, the enhancement in all these three efficiencies is required.

$$EQE = IQE \times IE \times LEE \quad (1)$$

The definitions of these efficiencies are summarized in Table 1. It is noted that here IQE is a measure of material quality, which is equivalent to radiative recombination efficiency. Factors that affect IQE include the defect density of materials, the strain state of the active region, quantum well design, and so on;[1] factors that affect IE include doping concentrations in materials, device structure design such as quantum wells, electron blocking layers, among others; and factors that affect LEE include the optical properties of materials, overall device design, metal contacts, and etc.

Table 1. Definition of efficiencies

Efficiency	Definition
EQE	$\eta_{EQE} = \frac{\text{number of photon emitted into free space per second}}{\text{number of electrons injected into LED per second}}$
IQE	$\eta_{IQE} = \frac{\text{the number of photons emitted from active region per second}}{\text{the number of electrons injected into active region per second}}$
IE	$\eta_{IE} = \frac{\text{number of electrons injected into active region per second}}{\text{number of electrons injected into the LED per second}}$
LEE	$\eta_{LEE} = \frac{\text{number of photons emitted into free space per second}}{\text{number of photons emitted from active region per second}}$

1.3. Objectives of this thesis

In this thesis, the focus is on IQE and LEE of AlGaN nanowire-based LEDs. Regarding IQE, as compared to the comprehensive studies of IQE for AlGaN quantum wells, studies on the IQE of AlGaN nanowires are much less. In this thesis, a systematic study on the Al content dependent and excitation dependent IQE at room temperature, which involves both experimental measurements and theoretical analysis, is carried out, aiming to have a fundamental understanding of the IQE of AlGaN nanowires as well as to improve IQE.

The thesis further investigates the LEE of AlGaN nanowire deep UV LEDs on Si through theoretical modeling. This is mainly motivated by several factors: 1) The LEE of conventional c-plane devices in the deep UV range, in particular for wavelengths close to 200 nm, has remained low. For example, the LEE of AlGaN quantum well LEDs emitting around 220 nm is only 1% or less.[32, 33] It is also noted that the light trapped inside the structure can also lead to heating effect and device instability.[34] The low LEE is largely limited by the intrinsic optical polarization switching from transverse-electric (TE) dominant to transverse-magnetic (TM) dominant as Al composition increases.[1, 35, 36] 2) Recent studies have shown that by using nanowire structures, the vertical top surface light extraction can be enhanced, e.g., Ref. [35]. 3) There have been no studies of large area AlGaN nanowire deep UV LEDs emitting in this wavelength range. 4) Estimating LEE is not a straightforward process, as LEE is sensitive to microscopic parameters such as refractive index, layer structure, and surface morphology; and it is difficult to measure LEE directly by experiments.[20] As such, the LEE of AlGaN nanowires deep UV LEDs emitting at 225 nm with a square, hexagonal, and honeycomb lattice is investigated using finite-difference time-domain method (FDTD) in the thesis. Moreover, the corresponding photonic crystal band

structures are calculated to understand the underlying mechanism of the LEE enhancement in comparison to conventional c-plane devices.

1.4. Organization of this thesis

This thesis is organized as follows. Chapter 1 gives an overview of AlGaN nanowire UV LEDs including their performance, followed by the objectives of this thesis.

Chapter 2 provides a literature review of the mainstream growth techniques of AlGaN nanowires, namely, chemical vapor deposition (CVD), metalorganic chemical vapor deposition (MOCVD), MBE, and selective area growth (SAG).

Chapter 3 to Chapter 5 present three manuscripts that address the research objectives of the thesis stated in Chapter 1. Chapter 3 and Chapter 4 present two papers on the IQE study of AlGaN nanowires, published in *Journal of Vacuum Science & Technology B*. Moreover, in Chapter 3, an additional review of typical methods to estimating IQE is elaborated before presenting the manuscript. In Chapter 5, a paper published in *Journal of Nanophotonics*, which concerns the LEE of a complete AlGaN nanowire deep UV LEDs on Si substrate with the use of graphene as the top electrode, is presented. In addition, the current progress of light extraction in the UV range by using nanostructures is also described in Chapter 5. In Chapter 6, the conclusions and future work are discussed.

2. Overview of AlGaN Nanowire Growth

The growth of AlGaN nanowires can be realized by catalytic and non-catalytic approaches. In this section, we will take an overview of the typical growth techniques in the literature as well as their characteristics.

2.1. VLS and CVD approach

Vapor-liquid-solid (VLS) is a typical catalyst-assisted growth method to fabricate semiconductor nanowires, in which the liquid catalysts (e.g., Au or Ni) adsorb vapor and accelerate the chemical reaction of nanowire growth at the liquid-solid interface.[37] This method can precisely control the nanowire size and density by the catalyst nanodroplet density and size.[21] However, the nanowire growth is limited to a small temperature window where the catalyst is thermodynamically stable.[37] Moreover, the use of catalyst droplet is at the risk of contaminating the desired nanowires.[21]

Most CVD growth is based on the VLS mechanism, and it can be catalytic and catalyst-free. For instance, with Pd catalyst, AlGaN nanostructures can be synthesized using Al powder, Ga droplets, and ammonia (NH_3) on Si and sapphire, with controllable morphology by the growth duration and the NH_3 flow rate.[38] AlGaN nanowires with full composition range have also been realized by the self-catalytic CVD growth.[39] The molten Al-Ga droplets, as a result of desorbing Al vapor into Ga droplets, are considered as the catalyst to facilitate the AlGaN nanowire formation, following the VLS mechanism.[39]

2.2. MOCVD and HVPE approach

This epitaxy technique involves using chemical compounds that contain the elements required for the material growth. Depending on if metalorganic compounds

are used as precursors, this approach can be further categorized into MOCVD and hydride vapor phase epitaxy (HVPE). For example, in HVPE method, GaCl and NH_3 can be used as Ga- and N-precursors, respectively;[40] whereas in MOCVD approach, trimethylgallium (TMGa) or triethylgallium (TEGa) serves as the Ga-source. During the reaction, the precursor gases are brought into a reactor together with a carrier gas (e.g., hydrogen (H_2) or nitrogen (N_2)). The precursors then undergo a pyrolysis process and leave subspecies to reside on the substrate surface for chemical reaction to occur, resulting in epitaxial semiconductor layers.

MOCVD growth technique also enables multiple quantum well (MQW) structure growth along the nonpolar direction, by utilizing the pulsed flow precursor method at the reduced growth pressure and growth temperature.[41, 42] The growth condition for MQWs has to be optimized in order to minimize the growth along semipolar/polar planes.[42] The period and thickness of MQWs can be tuned by varying the number of pulses.[41] Notably, core-shell MQW structures along the nonpolar m-plane have been demonstrated in AlGaN nanowires.[21] Shown in Fig. 2, a single core-shell AlGaN nanowire consists of an n-GaN core and a p-GaN shell with AlGaN cladding layers and MQWs sandwiched in between. The lateral stack of MQWs suppresses the polarization field and thus minimizes QCSE.[21]

Nonetheless, the growth of AlGaN nanowires occurs at a relatively high temperature above 1000 ℃ which is unfavorable for dopant incorporation and limits the selection of growth substrates.[5, 43, 44]

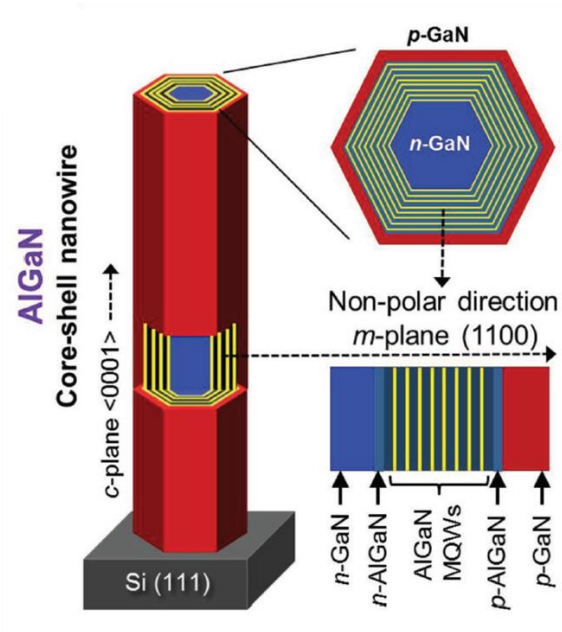

Fig. 2 Schematic of an AlGaN core-shell MQW nanowire; the MQWs are grown along the nonpolar m-plane.[21]

2.3. MBE approach

MBE has emerged as a favorable catalyst-free growth method for AlGaN nanowires.[37] This method takes place in ultra-high vacuum environment (i.e., ~10^{-10}–10^{-11} Torr), which ensures the highest material purity among all the growth approaches. The metal species are in solid form, such as Ga and Al for the AlGaN nanowire growth. The typical nitrogen supplies are NH_3 and N-plasma. The nitrogen radicals are obtained by thermal dissociation of NH_3 onto the substrate surface in the case of NH_3, whereas the radicals are created by electrically discharging nitrogen gas in the latter case.[37, 45]

During the growth, the solid precursors are heated in separate Knudsen diffusion cells or electron-beam evaporators until they begin to sublime slowly. The gaseous precursors then impinge on the substrate at certain atomic fluxes. The MBE growth of nanowires undergoes two stages: (1) nucleation stage and (2) post-nucleation stage.[37]

At the nucleation stage, the density of nanowires is defined. The density of binary alloys, such as GaN, can be better controlled by temperature and Ga flux than that of ternary alloys.[46] Therefore, in the context of the AlGaN nanowire growth, a GaN nanowire template layer is usually grown prior to the AlGaN layer to form a base for the subsequent nanowire growth.[9, 46]

With this technique, apart from Si substrate, AlGaN nanowires on unconventional substrates, such as metal thin films and metal-coated substrates, have also been demonstrated. May et al. have presented MBE-grown AlGaN nanowires on bulk metallic glass and Pt metal films, which improve the nanowire uniformity and partially reflect the light from the surface.[47] Sarwar et al. have reported AlGaN nanowire UV LEDs on Ti and Mo films with a promising prospect for large scale fabrication.[18]

2.4. SAG approach

SAG involves a thin layer of growth mask on the substrate. The mask layer with periodic nanoholes is patterned by standard e-beam lithography and reactive ion etching.[34, 48] The patterned substrate is then transferred into the MBE growth chamber or MOCVD reactor for the subsequent AlGaN nanowire growth.[34, 48, 49] This method allows the as-grown nanowires with uniform and well-defined radius, spacing and spatial arrangement, as shown by Fig. 3. As the nanohole radius and periodicity are pre-defined prior to the nanowire growth, SAG approach can thus enable a much thicker and sparser nanowire matrix compared to the spontaneous growth. AlGaN nanowires with almost a whole Al composition range grown by SAG are demonstrated by Prof. Mi's group.[34] The maximum room-temperature IQE of these nanowires is up to 45%.[34]

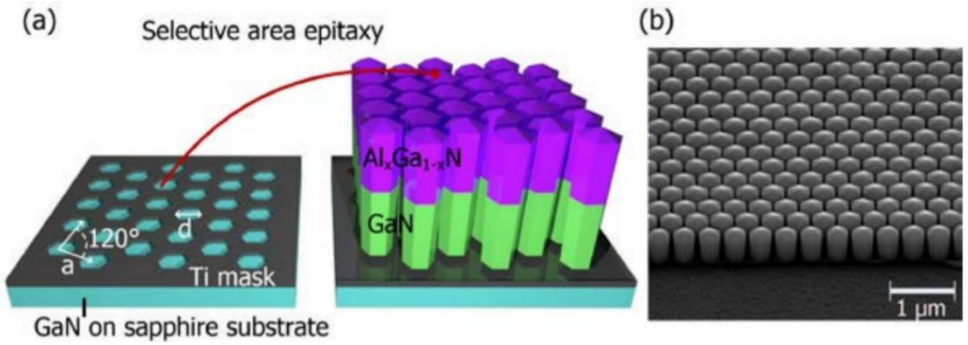

Fig. 3 (a) Schematic of SAG of AlGaN nanowires on GaN nanowire template. (b) An SEM image of AlGaN nanowires on GaN nanowire template grown by SAG.[34]

3. Optical Characterization of AlGaN Nanowires with Varying Al Contents

In this chapter, the optical properties of AlGaN nanowires with varying Al compositions grown by MBE are studied in detail. The study reveals excitation dependent IQE with varying Al contents. An overview of typical methods to estimate IQE and their limitations is also presented.

3.1. PL measurement for estimating internal quantum efficiency

Photoluminescence (PL) is a process wherein the emission of light is caused by the absorption of incoming photons by the material. The PL measurement is commonly used to estimate the IQE of semiconductor materials. Today, three methods are typically used for estimating the room-temperature IQE through PL experiments.

Method 1

In this method, the excitation power dependent PL spectra are measured at both low temperature and room temperature, and from which the power dependent relative PL efficiency can be derived by the ratio of PL intensity to the excitation power. By further assuming the maximum relative PL efficiency at low temperature to be 100% (i.e., IQE = 100%), the room-temperature power dependent IQE can be estimated by taking the ratio of the relative PL efficiency under different excitations at room temperature to the maximum relative PL efficiency at low temperature. This is shown in Fig. 4(a). In Fig. 4(a), we have to point out the prominent decreasing trend of IQE at high excitations. This decrease can be associated with the high carrier density related nonradiative recombination mechanism, i.e,. Auger recombination which is a three-carrier recombination process involving the energy transfer from an electron-hole pair

to the third free electron.[23, 50]

Nonetheless, by assuming the maximum relative PL efficiency to be 100%, the nonradiative recombination centers are considered completely frozen at low temperature.[20] This assumption, however, is not necessarily valid.[51]

Method 2

This method is based on the temperature-dependent PL measurements under a given excitation power. Shown in Fig. 4(b) is the integrated PL intensity as a function of the temperature.[34] The room-temperature IQE is estimated through dividing the room-temperature integrated PL intensity by the integrated PL intensity at the lowest temperature in the measurement.

The limitations of this approach include: 1) The temperature-dependent PL spectra are only measured at one excitation power, and thus the excitation dependent IQE cannot be determined at room temperature. 2) This method assumes the low-temperature IQE to be 100% for any excitation in the measurement. However, the IQE is excitation dependent at low temperature. 3) Following 2), this method could lead to an overestimation and/or an underestimation of the room-temperature IQE.

Method 3

In this method, the excitation dependent PL measurements are carried out at room temperature and low temperature under the same excitation powers. The room-temperature IQE is estimated by taking the ratio of the room-temperature integrated PL intensity and the low-temperature integrated PL intensity under the same excitation powers, as exampled in Fig. 4(c).[8, 24]

This method assumes 100% IQE at low temperature for all excitation powers in the

measurement, despite the fact that IQE is excitation dependent at low temperature. Moreover, similar to Method 2, this method could also lead to an overestimation and/or a underestimation of the room-temperature IQE, and thus an erroneous IQE trend as a function of the excitation power at room temperature.[52]

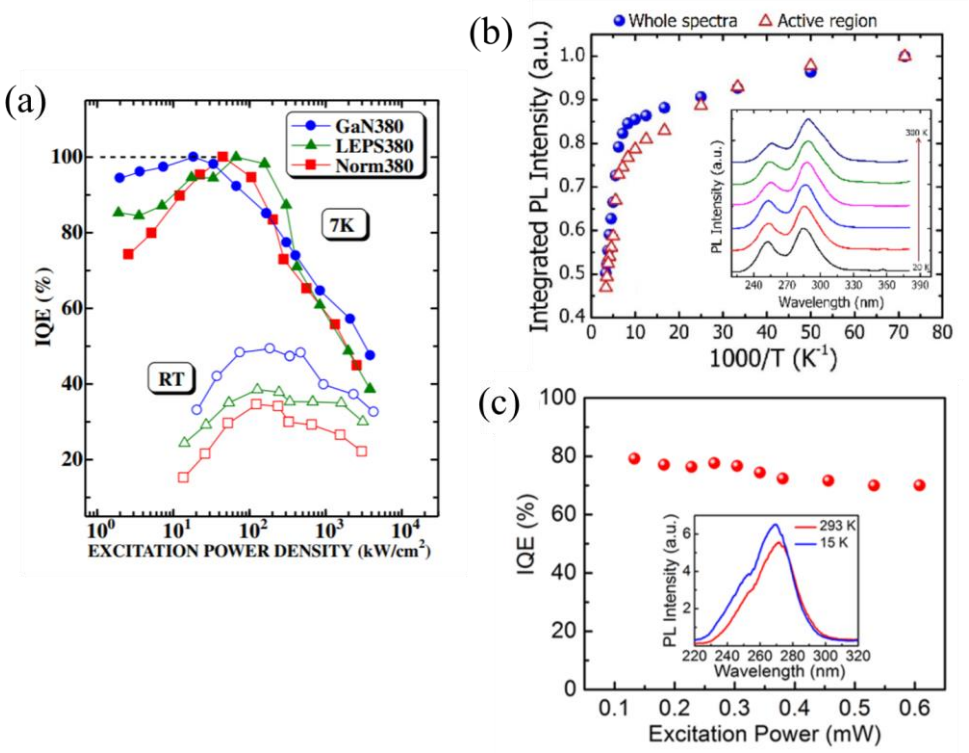

Fig. 4 (a) IQE of GaN layer as a function of the excitation power density at 7 K and room temperature.[51] © 2012 The Japan Society of Applied Physics. (b) Temperature-dependent integrated PL intensity measured from 14 K to 300 K at 50 mW for the AlGaN active region.[34] (c) IQE of AlGaN tunnel junction nanowire LED structures under different excitation powers.[24]

3.2. Manuscript

The following manuscript studies the optical properties of AlGaN nanowires grown under varying Al fluxes. It focuses on a fundamental understanding of Al composition and excitation dependent IQE of AlGaN nanowires in deep UV wavelengths. The manuscript is formatted as the journal's submission template.

The intrinsic excitation-dependent room-temperature internal quantum efficiency of AlGaN nanowires with varying Al contents

Jiaying Lu, Yun Zhong, and Songrui Zhao*

Department of Electrical and Computer Engineering, McGill University, 3480 University Street, Montreal, Quebec H3A 0E9, Canada
Electronic mail: songrui.zhao@mcgill.ca

Aluminum gallium nitride (AlGaN) nanowires have become an emerging approach for semiconductor deep ultraviolet light-emitting devices. To further improve the device performance, it is critical to understand the optical quality of AlGaN nanowires. However, today the room-temperature internal quantum efficiency (IQE) of AlGaN nanowires is predominantly analyzed by the temperature-dependent photoluminescence (PL) approach under one excitation power or taking the PL intensity ratio at the room temperature and low temperature with different excitation powers. In both cases, one needs to assume the low temperature IQE to be 100%, which is not always valid, in particular when the excitation power changes at the low temperature. In this work, we study the room-temperature IQE of AlGaN nanowires through the detailed excitation power-dependent PL experiments and theoretical analysis. This allows us to derive the intrinsic room-temperature IQE of AlGaN nanowires as a function of the excitation power. It is found that for an Al content in the range of 22% to 54%, the IQE of all samples increases as the excitation increases, followed by an efficiency droop. Moreover, comparing different samples, the IQE at low excitations increases as the Al content increases, whereas the peak IQE reduces from 73% to 56% as the Al content increases. The underlying mechanisms are also discussed in this paper.

I. INTRODUCTION

In recent years, aluminum nitride gallium (AlGaN) nanowires have emerged as an appealing route for the development of semiconductor deep ultraviolet (UV) light-emitting devices [1-4]. Noticeably, with the improved understanding of the molecular beam epitaxy (MBE) growth of GaN and AlGaN nanowires in the past [5-10], the deep UV light-emitting devices based on the MBE-grown AlGaN nanowires have shown performance characteristics comparable to conventional AlGaN quantum well deep UV light-emitting devices [11-18]. For example, lasing under the electrical injection in the deep UV band has been reported [14, 15, 19]. Moreover, AlN nanowire deep UV light-emitting diodes (LEDs) have shown drastically improved I-V characteristics compared to AlN thin film LEDs, benefited from the dopant incorporation in nanowire structures [11, 20, 21].

To further improve the performance of AlGaN nanowire deep UV light-emitting devices, a thorough understanding of the optical quality of AlGaN nanowires is required. Nonetheless, compared with the diverse and comprehensive studies on the optical quality of AlGaN epilayers and quantum wells [22-31], the studies on the optical quality of AlGaN nanowires have been much less. For example, the predominant approach of examining the room-temperature internal quantum efficiency (IQE) of AlGaN nanowires is to use the ratio of the photoluminescence (PL) intensity at the room temperature and low temperature, e.g., Refs. 5, 9, and 11. In such an approach, it is often assumed that the low-temperature IQE is unity, which, however, is not always valid [32]. Moreover, as the IQE is a function of the excitation power, taking the ratio becomes not straightforward. Our recent studies have also shown that such an approach tends to *overestimate* the room-temperature IQE, due to the presence of the efficiency droop at low temperature as the excitation increases [33]. It is thus necessary to derive the intrinsic room-temperature IQE of AlGaN nanowires as a function of the excitation

power.

Here, we investigate the IQE of AlGaN nanowires, with the Al content varying from 22% to 54%, through the detailed PL experiments and theoretical analysis. By analyzing the room-temperature excitation-power dependent PL intensity with a theoretical model involving the first-order nonradiative recombination (An) and the higher-order nonradiative recombination (Cn^3), as well as the bimolecular radiative recombination (Bn^2), where A, B, and C are the respective recombination coefficients and n is the carrier density, we derived the intrinsic room-temperature excitation-dependent IQE of AlGaN nanowires with different Al contents. It is found that at low excitations the IQE increases as the Al content increases, which could be mainly attributed to a combined effect of the formation of the Al-rich AlGaN shell and carrier localization due to compositional fluctuation. On the other hand, the efficiency droop is measured from all the samples, and the peak IQE reduces from 73% to 56% as the Al content increases. The underlying mechanism for the efficiency droop could be due to carrier delocalization, saturation of the radiative recombination, and Auger recombination.

II. EXPERIMENTAL

In this work, all the samples were grown by radio-frequency (RF) plasma-assisted MBE on Si (111) substrates. The Si wafers were cleaned by standard solvents, followed by hydrofluoric acid to remove surface oxide, prior to loading to the MBE chamber. Before the growth of AlGaN nanowires, GaN nanowires were grown first as the template. The substrate temperature was calibrated using the Si (111) 1×1 to 7×7 surface reconstruction during the ramping up of the substrate temperature. The detailed

growth conditions included a nitrogen flow rate of 1 sccm, a RF plasma power of 350 W, a substrate temperature for GaN layer of 745 ℃, a substrate temperature for AlGaN layer of 785 ℃, and a Ga flux of 4.0×10^{-8} Torr. The Al flux was varied, as shown in **Table I**, to change the alloy composition. Sample A - E correspond to the sample with the lowest Al content to the sample with the highest Al content. The thicknesses of the GaN nanowire segment and the AlGaN nanowire segment for all the samples in this work are around 500 nm and 200 nm, respectively.

TABLE I. The Al content and the corresponding Al flux for Sample A - E, as well as key parameters used in the PL analysis for deriving the IQE of these samples.

Sample	Al flux (Torr)	Al content	Fill factor (FF)	Refractive index	Fresnel reflection (R_F)	Parameter γ as in Eq. (1) ($\times10^{-24}$)
A	1.2×10^{-8}	0.22	0.583	2.60	7.63 %	1.72079
B	1.8×10^{-8}	0.28	0.659	2.60	9.51 %	2.33321
C	2.7×10^{-8}	0.35	0.705	2.58	10.58 %	3.84611
D	4.2×10^{-8}	0.42	0.720	2.56	10.82 %	5.39733
E	6.4×10^{-8}	0.54	0.799	2.50	12.43 %	2.43687

The scanning electron microscope (SEM) images of Sample A to E are shown by **Figures 1(a) - 1(e)**, respectively, which were all taken at a 45° tilting angle. It is seen that relatively uniform and vertically aligned nanowires are formed. Further detailed examination indicates an increased fill factor (FF) as the Al content increases. The estimated FF values for different samples are also shown in **Table I**.

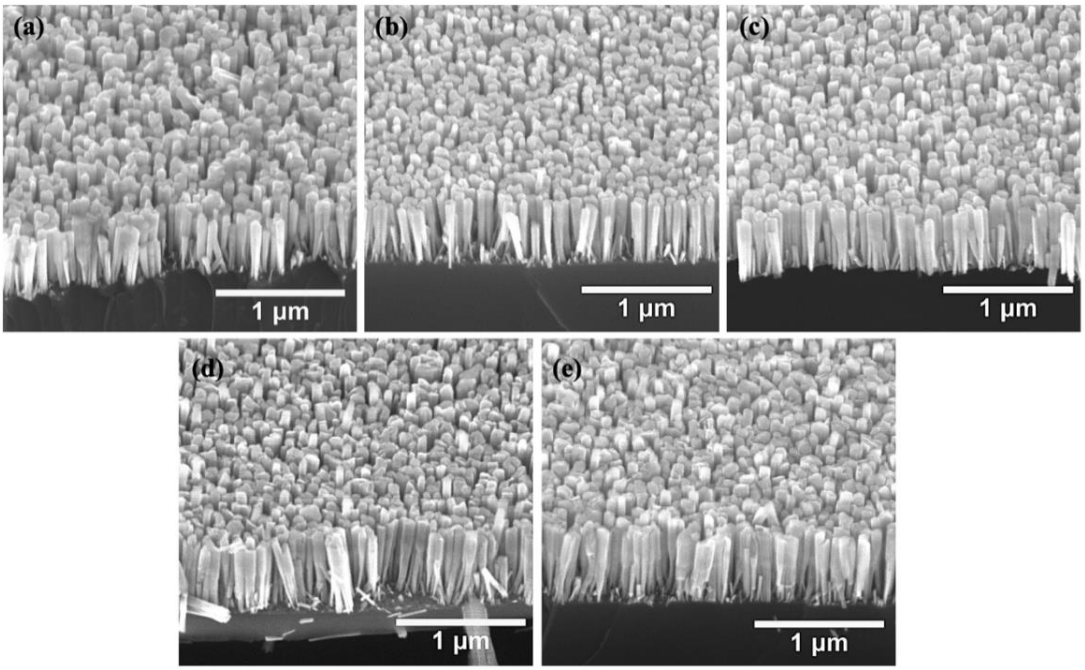

FIG. 1. (a)-(e) SEM images of AlGaN nanowires from the lowest Al composition to the highest Al composition (Sample A to E).

The room-temperature power-dependent PL experiments were performed using a 213 nm solid-state laser, with a pulse width of 7 ns. The estimated spot size illuminating on the sample surface was approximately 0.09 mm^2. The laser beam was focused onto the sample surface by a silica focus lens, and the emitted light was also collected from the sample surface by a silica focus lens and then directed to a deep UV spectrometer.

III. RESULTS AND DISCUSSION

The room-temperature PL spectra measured from Sample A - E under an excitation of 7.9 $kW \cdot cm^{-2}$ are shown in **Figure 2**. The PL spectra are normalized to the peak intensity for each sample. It is seen that by changing Al contents, PL emission

from 260 nm to 320 nm can be obtained. The Al contents for all samples were further estimated via $E_g(x) = E_g^{AlN}x + E_g^{GaN}(1-x) - bx(1-x)$ and are shown in **Table I**. In this estimation, $E_g^{AlN} = 6.2\ eV$, $E_g^{GaN} = 3.4\ eV$ (at 300 K), the bowing factor b was assumed to be 0.7 eV [34], and it was further assumed that the PL peak energy is close to the bandgap energy under the excitation of 7.9 kW·cm^{-2}.

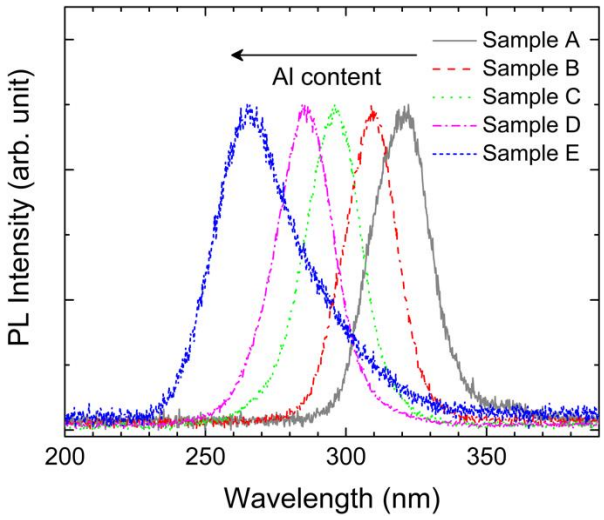

FIG. 2. The normalized PL spectra from Sample A (lowest Al content) to E (highest Al content) under an excitation of 7.9 kW·cm^{-2} at the room temperature.

The power-dependent PL emission was further measured from Sample A - E, through which the power-dependent integrated PL intensity (I_{PL}) can be obtained. The I_{PL} as a function of the excitation power density for Sample A - E in a logarithmic scale is shown in **Figure 3**. Solid lines with a slope $k = 1$ and dashed lines with a slope $k = 2$, which correspond to the radiative recombination dominated process and the first-order nonradiative recombination dominated process, respectively, are also shown in **Fig. 3**. The onset of the slope $k = 1$ is marked by an arrow. Comparing Sample A - E, it is seen that the onset shifts to lower excitations as the Al content increases, suggesting that the radiative recombination becomes dominant at lower excitations as the Al content increases and thus an increase of IQE at low excitations as the Al content increases. In

addition, the slope k reduces to less than 1 at high excitations (more noticeable for Sample B - E), hinting a decrease of IQE at high excitations. Moreover, the deviation from the slope $k = 1$ (marked by *) shifts to lower excitations as the Al content increases, hinting that the peak IQE also shifts to lower excitations as the Al content increases.

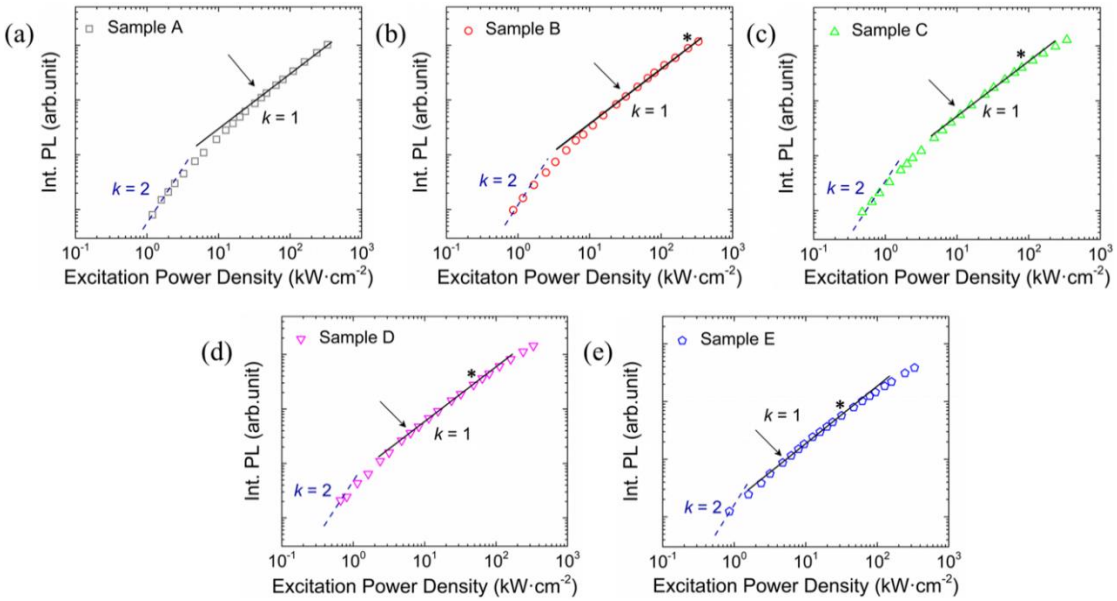

FIG. 3. (a)-(e) I_{PL} as a function of the peak power density in a logarithmic scale for the AlGaN nanowires from the lowest Al content to the highest Al content (Sample A to E). The dash and solid lines, which indicate the first-order nonradiative recombination and the radiative recombination, respectively, are also annotated. The arrows mark the onset of the slope $k = 1$, and the symbol * denotes the onset of the deviation from the slope $k = 1$.

We next describe the theoretical model to analyze the excitation-dependent IQE using I_{PL}. Under the steady state approximation, the generation rate G is equal to the recombination rate R, i.e., $G = R$. Further taking account the major channels involved in the carrier recombination processes, including the first-order nonradiative recombination An, the bimolecular radiative recombination Bn^2, and the higher-order nonradiative recombination Cn^3, G can be expressed as $G = R = An+Bn^2+Cn^3$. Further

expressing I_{PL} in the following form,

$$I_{PL} = \gamma B n^2, \tag{1}$$

where I_{PL} is experimentally determined as described earlier and γ is an experimental parameter mainly determined by the excitation volume and the total PL collection efficiency, we have,

$$G = \frac{A}{\sqrt{B\gamma}}\sqrt{I_{PL}} + \frac{1}{\gamma} I_{PL} + \frac{C}{\sqrt{(B\gamma)^3}}\sqrt{{I_{PL}}^3}, \tag{2}$$

Separately, G can be determined experimentally via,

$$G = \frac{P_{laser}(1 - R_F)\alpha}{A_{spot} h\nu}, \tag{3}$$

where P_{laser} is the peak excitation power, R_{F} is the Fresnel reflection, α is the absorption coefficient, A_{spot} is the area of the laser beam incident on the sample, and $h\nu$ is the photon energy of the laser. The value of R_{F} was calculated using the Fresnel's law, wherein the effective refractive index of the nanowire-air composite was determined by the Maxwell-Garnett equation. The Al content-dependent refractive indices are shown in **Table I**. The calculated R_{F} values are also shown in **Table I**. For Sample A to E, the absorption coefficient α was estimated to be 25, 25, 23.5, 20, 15 μm^{-1}, respectively [35].

Therefore, with the experimentally determined $I_{\text{PL}} - P_{\text{laser}}$ dependence and Eq. (3), one can obtain the experimental $G - I_{\text{PL}}$ dependence, which can be further fitted by Eq. (2). This will allow one to determine γ (shown in **Table I**) through fitting, and IQE can be further calculated via,

$$\text{IQE} = \frac{Bn^2}{An + Bn^2 + Cn^3} = \frac{I_{PL}}{\gamma \cdot G}. \tag{4}$$

At this point, it is important to know that the calculated IQE is independent on the choice of the A, B, and C coefficients and thus reflects the intrinsic room-temperature IQE as a function of the excitation power for the present AlGaN nanowires if a good

fitting is obtained. **Figure 4** shows the experimentally determined $G - I_{PL}$ dependence, together with the fitting curves using Eq. (2). It is seen that excellent fittings can be obtained.

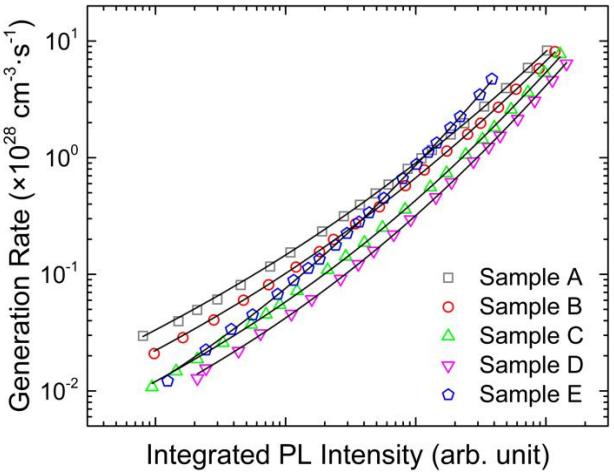

FIG. 4. G vs. I_{PL} for the AlGaN nanowires with different Al contents. The solid lines are the fitting curves based on Eq. (2).

Figure 5 shows the calculated room-temperature IQE as a function of the generation rate G. It is seen that at low excitations, e.g., at a generation rate of 3×10^{26} $cm^{-3}\cdot s^{-1}$, the IQE increases as the Al content increases, with the sample of the highest Al content showing an IQE of 46%. This Al content-dependent IQE is in contrast to the previous studies in AlGaN quantum wells, wherein it is proposed that the IQE at low excitations is only determined by the threading dislocation density (TDD) and is not dependent on the Al content [24]. This trend, on the other hand, is similar to what is found in AlGaN epilayers [29,31] as well as in AlGaN nanowires with a similar Al content range [9], although in these studies the IQE was estimated by the ratio of PL intensities at the room temperature and low temperature.

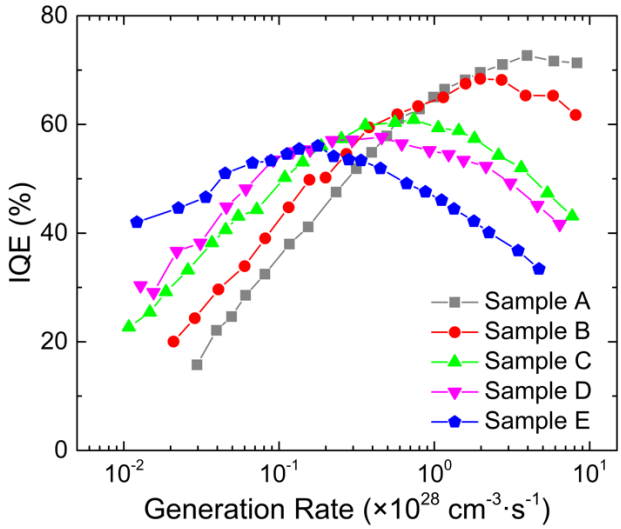

FIG. 5. The calculated room-temperature IQE as a function of the generation rate *G* for the AlGaN nanowires with different Al contents.

In the previous studies [9, 29, 31], the increased IQE with the increase of the Al content is ascribed to the carrier localization effect due to alloy fluctuations and/or compositional inhomogeneity. Indeed, for AlGaN nanowires grown with similar conditions as in the present study, strong compositional fluctuation was found [19]; hence, the carrier localization could be the mechanism to explain the increased IQE as the Al content increases in the present study.

Nonetheless, another mechanism could also contribute to the increased IQE as the Al content increases, i.e., the formation of Al-rich AlGaN shell. The formation of Al-rich AlGaN shell in AlGaN nanowires has been reported, which is generally considered to be kinetics driven [5, 9, 16, 19]; and such an effect is found to be more pronounced in AlGaN nanowires with higher Al contents [5]. The Al-rich AlGaN shell can passivate the nanowire surface and minimize the adverse effects of surface defects and/or states, such that IQE can be improved at low excitations. Previously, the improved IQE of visible-color emitting InGaN/AlGaN nanowire structures, due to the formation of AlGaN shell, has been reported [36].

We further estimated the IQE at low carrier densities (e.g., 1×10^{18} cm^{-3}) of different samples. In our IQE analysis with Eq. (4), we have bypassed the *A*, *B*, and *C* coefficients. To further determine the recombination coefficients, a separate evaluation, i.e., the time-resolved PL, is required, which can determine the *B* coefficient, such that *A* and *C* can be further determined [37]. Recent studies suggest that, by considering the compositional fluctuation induced carrier localization effect, the *B* coefficient increases as the Al content increases [29] and is different between quantum wells and bulk materials [30]. If following Ref. 29 and taking the bulk *B* coefficient at similar Al contents, i.e., 1.6×10^{-11}, 1.8×10^{-11}, 2.4×10^{-11}, 3.2×10^{-11}, and 5×10^{-11} $cm^3\cdot s^{-1}$ for Sample A - E, the carrier density for each sample can be calculated by $I_{PL} = \gamma Bn^2$; and thus the IQE at a carrier density of 1×10^{18} cm^{-3} can be further derived, which increases from 10% to 37% from Sample A - E.

We next discuss the IQE at high excitations. From **Figure 5**, it is seen that for all the samples, the IQE increases as the generation rate increases, followed by a decrease (more noticeable from Sample B - E). Furthermore, the peak IQE reduces as the Al content increases, with the sample of the lowest Al content showing the highest peak IQE (73%) and the sample of the highest Al content showing the lowest peak IQE (56%). Moreover, the peak IQE shifts to lower excitations as the Al content increases.

This IQE trend resembles what is measured in the previous studies on the excitation-dependent efficiency droop of AlGaN epilayers with different Al contents, wherein the carrier delocalization is proposed to be the underlying mechanism [31]. Further considering the presence of compositional fluctuations in the AlGaN nanowires, the carrier delocalization thus could be a possible mechanism for the efficiency droop behavior. Moreover, in the present study, due to the use of pulsed laser excitation, heating effect is not likely the cause. However, in the present study, we could not

examine other mechanisms such as saturation of the radiative recombination due to phase space filling and Auger recombination, which might be additional causes for the efficiency droop.

In the end, it is worth pointing out that the IQE derived in the present study might represent the lower bound. First, although the emission from the GaN segment is barely detectable at low excitations, it is measurable at high excitations (the intensity is 1-2 orders of magnitude lower compared to the emission intensity from the AlGaN segment); as such, the IQE at high excitations is underestimated. Second, although the use of the relative thick AlGaN segment can mitigate issues related to thin AlGaN quantum wells (e.g., carrier diffusion and/or transport effects from other undesirable layers to the well, the light absorption from other undesirable layers) [27, 28], it makes the excitation power reduces as the light penetrates deeper, such that the effective generation rate might be lower across the whole AlGaN segment compared to the calculation using Eq. (3), and thus the IQE is underestimated. Nonetheless, it is noted that different from epilayers wherein the excitation purely depends on the penetration process, for nanowires the laser light can excite the lower portion via the nanowire sidewall, through a scattering process. Lastly, it is also worth mentioning that these variations do not affect the comparison among different samples, as the influence is similar to all the samples.

IV. SUMMARY AND CONCLUSIONS

In conclusion, we have derived the room-temperature excitation-dependent IQE of AlGaN nanowires with Al contents varying from 22% to 54%. In this Al content range, it is found that at low excitations, the IQE increases as the Al content increases. The

increased IQE as the Al content increases at low excitations could be related to a combined effect of the formation of the Al-rich AlGaN shell and carrier localization due to compositional fluctuations. Efficiency droop is also measured, and the peak IQE shows an Al content dependence, i.e., the peak IQE reduces from 73% to 56% as the Al content increases. The underlying mechanism for the droop could be related to the carrier delocalization; however, other mechanisms such as the saturation of the radiative recombination and Auger recombination could be additional causes.

ACKNOWLEDGMENTS

This work is supported under Natural Sciences and Engineering Research Council of Canada (NSERC) RGPIN-2019-04726, NSERC DGECR-2019-00494, and McGill University.

DATA AVAILABILITY STATEMENT

The data that supports the findings of this study are available within the article.

Further reasonable request can be made to the corresponding author.

Reference

[1]C. Zhao, N. Alfaraj, R. Chandra Subedi, J. W. Liang, A. A. Alatawi, A. A. Alhamoud, M. Ebaid, M. S. Alias, T. K. Ng and B. S. Ooi, Prog. Quant. Electron. **61**, 1-31 (2018).

[2]S. Zhao, J. Lu, X. Hai and X. Yin, Micromachines (Basel) **11**, 125 (2020).

[3] J. W. Min, D. Priante, M. Tangi, G. Liu, C. H. Kang, A. Prabaswara, C. Zhao, L. Al-

Maghrabi, Y. Alaskar, A. M. Albadri, A. Y. Alyamani, T. K. Ng and B. S. Ooi, J. Nanophotonics **12**, 043511 (2018).

[4]S. Zhao and Z. Mi, IEEE J. Quantum Electron. **54**, 1-9 (2018).

[5]A. Pierret, C. Bougerol, S. Murcia-Mascaros, A. Cros, H. Renevier, B. Gayral and B. Daudin, Nanotechnology **24**, 115704 (2013).

[6]K. A. Bertness, N. A. Sanford and A. V. Davydov, IEEE J. Sel. Top. Quant. Electron. **17**, 847 (2011).

[7]E. Calleja, J. Ristić, S. Fernández-Garrido, L. Cerutti, M. A. Sánchez-García, J. Grandal, A. Trampert, U. Jahn, G. Sánchez, A. Griol and B. Sánchez, Phys. Status Solidi (B) **244**, 2816-2837 (2007).

[8]H. Sekiguchi, K. Kato, J. Tanaka, A. Kikuchi and K. Kishino, Phys. Status Solidi (A) **205**, 1067-1069 (2008).

[9]C. Himwas, M. den Hertog, L. S. Dang, E. Monroy and R. Songmuang, Appl. Phys. Lett. **105**, 241908 (2014).

[10]S. Zhao, S. Y. Woo, S. M. Sadaf, Y. Wu, A. Pofelski, D. A. Laleyan, R. T. Rashid, Y. Wang, G. A. Botton and Z. Mi, APL Mater. **4**, 086115 (2016).

[11]S. Zhao, A. T. Connie, M. H. Dastjerdi, X. H. Kong, Q. Wang, M. Djavid, S. Sadaf, X. D. Liu, I. Shih, H. Guo and Z. Mi, Sci. Rep. **5**, 8332 (2015).

[12]H. Sun, M. K. Shakfa, M. M. Muhammed, B. Janjua, K.-H. Li, R. Lin, T. K. Ng, I. S. Roqan, B. S. Ooi and X. Li, ACS Photonics **5**, 964-970 (2017).

[13]S. M. Sadaf, S. Zhao, Y. Wu, Y. H. Ra, X. Liu, S. Vanka and Z. Mi, Nano Lett. **17**, 1212-1218 (2017).

[14]S. Zhao, X. Liu, Y. Wu and Z. Mi, Appl. Phys. Lett. **109**, 191106 (2016).

[15]S. Zhao, X. Liu, S. Y. Woo, J. Kang, G. A. Botton and Z. Mi, Appl. Phys. Lett. **107**, 043101 (2015).

[16]K. H. Li, X. Liu, Q. Wang, S. Zhao and Z. Mi, Nat Nanotechnol **10**, 140 (2015).

[17]S. Zhao, S. M. Sadaf, S. Vanka, Y. Wang, R. Rashid and Z. Mi, Appl. Phys. Lett. **109**, 201106 (2016).

[18]S. D. Carnevale, T. F. Kent, P. J. Phillips, M. J. Mills, S. Rajan and R. C. Myers, Nano Lett. **12**, 915-920 (2012).

[19]S. Zhao, S. Y. Woo, M. Bugnet, X. Liu, J. Kang, G. A. Botton and Z. Mi, Nano Lett. **15**, 7801-7807 (2015).

[20]S. Zhao, M. Djavid and Z. Mi, Nano Lett. **15**, 7006 (2015).

[21]A. M. Siladie, G. Jacopin, A. Cros, N. Garro, E. Robin, D. Caliste, P. Pochet, F. Donatini, J. Pernot and B. Daudin, Nano Lett. **19**, 8357-8364 (2019).

[22]J. Yun, J.-I. Shim and H. Hirayama, Appl. Phys. Express **8**, 022104 (2015).

[23]Z. Bryan, I. Bryan, J. Xie, S. Mita, Z. Sitar and R. Collazo, Appl. Phys. Lett. **106**, 142107 (2015).

[24]K. Ban, J.-i. Yamamoto, K. Takeda, K. Ide, M. Iwaya, T. Takeuchi, S. Kamiyama, I. Akasaki and H. Amano, Appl. Phys. Express **4**, 052101 (2011).

[25]M. Shatalov, J. Yang, W. Sun, R. Kennedy, R. Gaska, K. Liu, M. Shur and G. Tamulaitis, J. Appl. Phys. **105**, 073103 (2009).

[26]K. Takeda, F. Mori, Y. Ogiso, T. Ichikawa, K. Nonaka, M. Iwaya, S. Kamiyama, H. Amano and I. Akasaki, Phys. Status Solidi (C) **7**, 1916-1918 (2010).

[27]F. Nippert, M. Tollabi Mazraehno, M. J. Davies, M. P. Hoffmann, H.-J. Lugauer, T. Kure, M. Kneissl, A. Hoffmann and M. R. Wagner, Appl. Phys. Lett. **113**, 071107 (2018).

[28]C. Frankerl, M. P. Hoffmann, F. Nippert, H. Wang, C. Brandl, N. Tillner, H.-J. Lugauer, R. Zeisel, A. Hoffmann and M. J. Davies, J. Appl. Phys. **126**, 075703 (2019).

[29]Ž. Podlipskas, R. Aleksiejūnas, A. Kadys, J. Mickevičius, J. Jurkevičius, G.

Tamulaitis, M. Shur, M. Shatalov, J. Yang and R. Gaska, J. Phys. D Appl. Phys. **49**, 145110 (2016).

[30]M. E. Rudinsky and S. Y. Karpov, Status Solidi (A) **217**, 1900878 (2019).

[31]J. Mickevičius, G. Tamulaitis, M. Shur, M. Shatalov, J. Yang and R. Gaska, Appl. Phys. Lett. **103**, 011906 (2013).

[32]J. B. Schlager, N. A. Sanford, K. A. Bertness and A. Roshko, J. Appl. Phys. **109**, 044312-044317 (2011).

[33]Y. Zhong, E. Berikaa, J. Lu, X. Yin and S. Zhao, AIP Adv. **10**, 025022 (2020).

[34]I. Vurgaftman and J. R. Meyer, J. Appl. Phys. **94**, 3675-3696 (2003).

[35]J. F. Muth, J. D. Brown, M. A. L. Johnson, Z. Yu, R. M. Kolbas, J. W. Cook and J. F. Schetzina, MRS Internet J. Nitride Semicond. Res. **4**, 502-507 (2014).

[36]H. P. T. Nguyen, M. Djavid, S. Y. Woo, X. Liu, A. T. Connie, S. Sadaf, Q. Wang, G. A. Botton, I. Shih and Z. Mi, Sci. Rep. **5**, 7744 (2015).

[37]Y. C. Shen, G. O. Mueller, S. Watanabe, N. F. Gardner, A. Munkholm and M. R. Krames, Appl. Phys. Lett. **91**, 141101 (2007).

4. Optical Characterization of AlGaN Nanowires on AlN Buffer Layer

In this chapter, a comparative study of optical quality of AlGaN nanowires grown on AlN buffer layer on Si and on bare Si substrate is presented.

4.1. Manuscript

The following manuscript studies the optical quality of AlGaN nanowires grown on AlN buffer layer. This work aims at improving AlGaN nanowire quality by employing a buffer layer. The manuscript is formatted as the journal's submission template.

A comparative study on the molecular beam epitaxial growth and characterization of AlGaN nanowire structures on AlN buffer layer and on Si

Jiaying Lu, Yun Zhong, and Songrui Zhao*

Department of Electrical and Computer Engineering, McGill University, 3480 University Street, Montreal, Quebec H3A 0E9, Canada
Electronic mail: songrui.zhao@mcgill.ca

AlGaN in the form of nanowires is an important platform for semiconductor ultraviolet light sources on Si. In the past, significant efforts have been devoted to improving the quality of AlGaN nanowires. In this context, we present a comparative study on the molecular beam epitaxial growth and characterization of AlGaN nanowire structures on AlN buffer layer on Si and on Si directly. It is found that AlGaN nanowires grown on AlN buffer layer shows an improved internal quantum efficiency (IQE), compared with the nanowires grown on Si directly. This improvement is attributed to the reduced nanowire coalescence due to the improved vertical alignment of the nanowires grown on AlN buffer layer.

I. INTRODUCTION

Semiconductor nanowires have received wide attention in the past for both fundamental science and device applications.[1] Among various semiconductor nanowires, aluminum gallium nitride (AlGaN) nanowires are of particular interest for the development of semiconductor deep ultraviolet (UV) light-emitting devices, which are an alternative to toxic mercury lamps for disinfections, water and air purifications,

and bio/chemical sensing [2]. The reasons of investigating AlGaN nanowires for UV light emitters are manifold: 1) large, direct, and tunable bandgap;[2] 2) better accommodation of the strains compared with thin films;[3] 3) the improved doping in nanowire structures;[4-7] and 4) the possibility of *in situ* integration of such UV light emitters on a wide range of substrates, including Si.[8-11] Over the past few years, significant progress has been made in AlGaN nanowire UV light-emitting devices on Si,[11] including AlGaN nanowire deep UV LEDs with sub-milliwatt to milliwatt light output powers on Si.[12, 13]

Such AlGaN nanowire deep UV LED structures are generally grown on Si (111) substrates by molecular beam epitaxy (MBE); and prior to the growth of the AlGaN segment, a GaN nanowire template is grown. Though having a great promise of this technology, an insulating silicon nitride (Si_xN_y) layer, which forms simultaneously during the nanowire growth process, is one of the remaining challenges. Such a layer impedes electrical conduction and heat dissipation, and also affects the vertical alignment of the nanowires with respect to the substrate. [10, 14] To overcome this issue, different strategies have been proposed, including using AlN buffer layers. [14-28] However, there have been neither detailed studies on the optical quality (i.e., internal quantum efficiency, IQE) of such AlGaN nanowire structures on AlN buffer layers nor a comparison to the IQE of AlGaN nanowire structures directly on Si.

It is further noted that, even for AlGaN nanowires grown on Si directly, the IQE requires a better understanding: In the previous studies, the temperature-dependent photoluminescence (PL) technique is often used to investigate IQE,[5, 12, 29, 30] wherein it

is assumed that the low-temperature IQE is 100%; this is, however, not necessarily a valid assumption. For example, our previous study on the optical properties of AlGaN nanowires shows that such an approach tends to give a *higher* room-temperature IQE due to the presence of efficiency droop at low temperatures as excitation increases.[31] This is in contrast to the numerous studies on AlGaN quantum wells that have provided a comprehensive understanding of the IQE, e.g., the carrier density dependence.[32, 33]

In this work, we present a comparative study on the molecular beam epitaxial growth and characterization of AlGaN nanowire structures emitting at a similar wavelength (~320 nm) on the AlN buffer layer on Si and on Si directly and unveil the correlated structural and optical properties of such nanowire structures. Through analysing the room-temperature power-dependent PL spectra using a theoretical model involving the first-order non-radiative recombination and higher-order non-radiative recombinations, as well as the bimolecular radiative recombination, we estimate the carrier density-dependent IQE. Comparing AlGaN nanowire structures on the AlN buffer layer to AlGaN nanowire structures on Si directly, the IQE at low carrier densities is improved, which is attributed to the improved nanowire vertical alignment and uniformity, as suggested by the statistical analysis on the nanowire size distribution.

II. EXPERIMENTAL

In this work, the AlGaN nanowires were grown by radio-frequency (RF) plasma-assisted MBE on Si (111) substrates. Prior to loading the wafer into the MBE

chamber, standard solvent cleaning, followed by hydrofluoric acid etching, was performed. The substrate temperature was calibrated using Si (111) 1×1 to 7×7 surface reconstruction during the ramping up of the substrate temperature. The AlGaN nanowires were grown on a GaN nanowire template. Before the growth of the GaN nanowire template, a thin AlN buffer layer (< 2 nm) was introduced using the Al-first approach, i.e., an AlN buffer layer was formed through firstly introducing Al and followed by nitridation.[22, 24, 25, 34-36] The subsequent growth of a GaN nanowire template was at a substrate temperature of 745℃, a nitrogen flow rate of 1 SCCM, and a Ga flux of 6.0×10^{-8} Torr. The AlGaN nanowire segments were grown at a substrate temperature of 785 ℃, a nitrogen flow rate of 1 SCCM, a Ga flux of 4.0×10^{-8} Torr, and an Al flux of 1.2×10^{-8} Torr. The growth durations for the GaN layer and the AlGaN layer were 2 h and 1 h, respectively. A similar growth condition was used for the growth of AlGaN nanowires on Si directly. As will be shown, both samples emit at a similar wavelength.

The room-temperature PL measurements were performed using a 213 nm laser to excite the sample. The laser light was focused onto the sample by a focus lens, and the emission from the sample was collected from the top surface with a focus lens, which was directed to a UV spectrometer.

III. RESULTS AND DISCUSSION

Figure 1(a) shows the RHEED pattern during the MBE growth of the AlGaN segment of the AlGaN nanowire structures on the AlN buffer layer. It is seen that well-

defined RHEED spots are observed, suggesting a well-aligned nanowire orientation with respect to the substrate.[14] This is in contrast to the AlGaN nanowires grown directly on Si substrates: shown in Fig. 1(b), a segmented concentric ring-like RHEED pattern is observed, indicating the disorientation of the grown nanowires with respect to the substrate. The improved nanowire vertical alignment is further supported by the scanning electron microscope (SEM) image: shown in Figs. 1(c) and 1(d), AlGaN nanowires grown on AlN buffer layer show a noticeably improved vertical alignment with respect to the substrate, compared with the nanowires grown directly on Si, which also leads to a more uniformity nanowire size distribution.

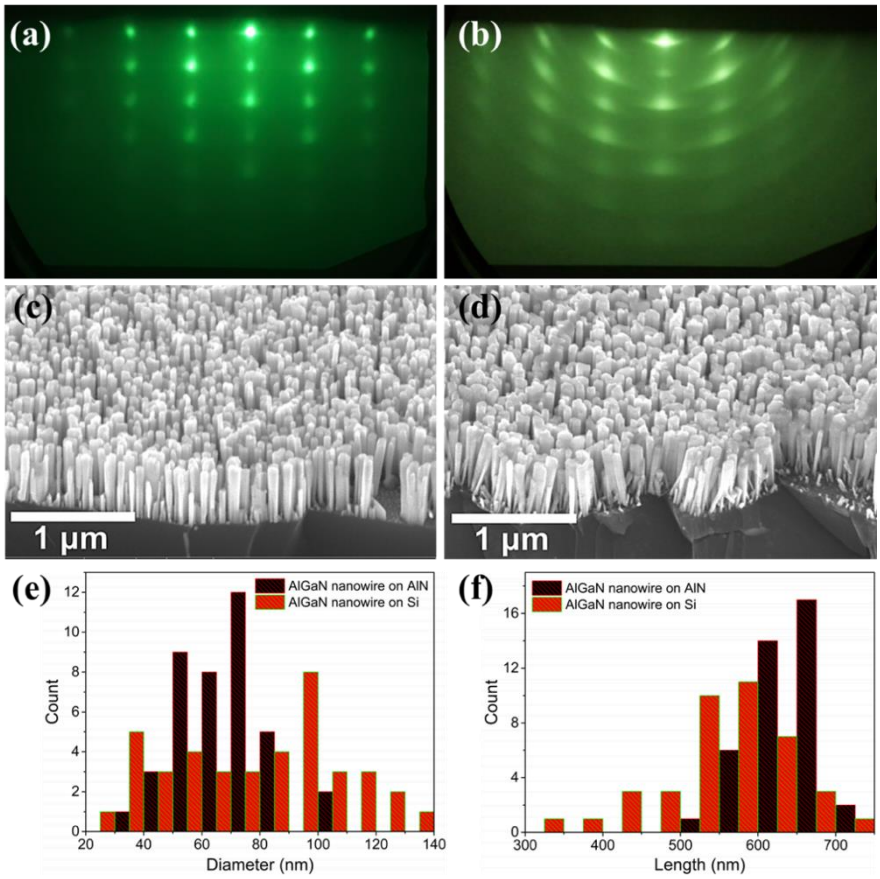

FIG. 1. (a) and (b) RHEED patterns captured during the growth of AlGaN nanowire structures on AlN buffer layer and on Si, respectively. (c) and (d) SEM images of the

AlGaN nanowire structures grown on AlN buffer layer and on Si, respectively. (e) and (f) statistical analysis of the nanowire diameter and the length based on SEM images for the AlGaN nanowire structures on AlN buffer layer and on Si.

Figures 1(e) and 1(f) show the detailed statistics of the nanowire size distribution for AlGaN nanowires grown on the AlN buffer layer and on Si directly. It is seen that the nanowires on the AlN buffer layer show a smaller variation regarding to both the diameter and length, compared with the nanowires on Si directly. The standard deviation of the nanowire length is 43 nm and 85 nm for the nanowires on AlN buffer layer and on Si, respectively. The standard deviation of the nanowire diameter is 14 nm and 29 nm for the nanowires on AlN buffer layer and on Si, respectively.

Detailed examinations further suggest that the nanowires grown on AlN buffer layer are mostly single-root, due to the improved vertical alignment. This is in contrast to the multiroot feature which is typically seen from the nanowires formed spontaneously on Si directly, regardless of growth condition.[31] The improved alignment can be ascribed to the suppression of the formation of Si_xN_y due to the use of the AlN buffer layer during the growth of the GaN nanowire template stage.[14]

We next investigated the room-temperature optical quality of AlGaN nanowires on AlN buffer layer and on Si by PL experiments. Figures 2(a) and 2(b) show the excitation-dependent PL spectra measured at the room temperature for the nanowires on the AlN buffer layer and on Si, respectively. It is seen that, at low excitations, only a peak around 320 nm is measured for both samples, whereas at high excitations, a second emission peak appears at around 360 nm for both samples. The two emission

peaks at around 320 nm and 360 nm correspond to the emission from the AlGaN segments and the GaN nanowires at the bottom, respectively. The average Al composition of both AlGaN layers is around 0.22. This number is estimated using Vegard's law, assuming the energy band gap of GaN and AlN is 3.4 eV and 6.2 eV, respectively. The dashed curves in Fig. 2 are Gaussian fittings, which are used to extract the integrated PL intensity (I_{PL}) associated with the AlGaN emission component under different excitation powers. The power-dependent I_{PL} is further used for IQE analysis as described below.

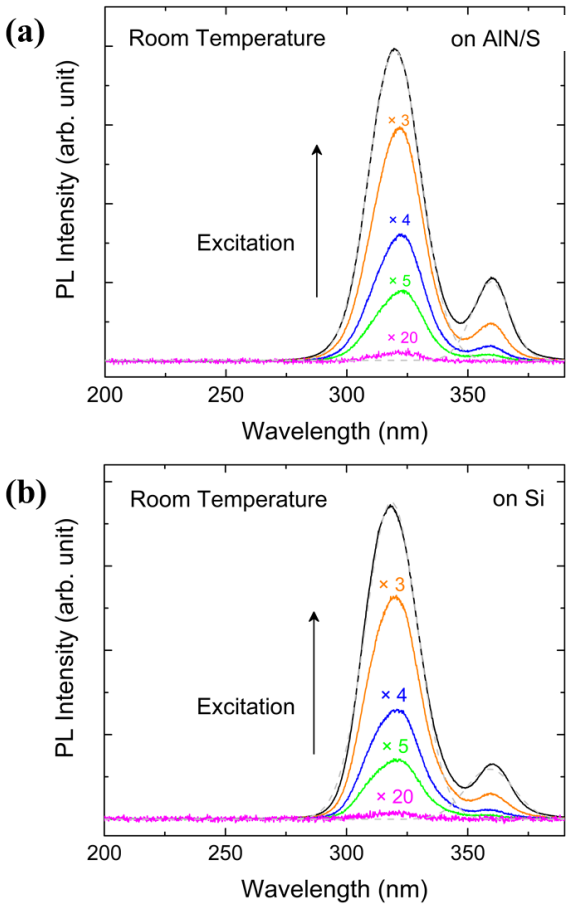

FIG. 2. (a) PL spectra of the AlGaN nanowire structures grown on the AlN buffer layer measured at room temperature, with excitations of 1, 16, 34, 80 and 340 kW·cm^{-2}. (b) The room-temperature PL spectra of the AlGaN nanowire structures grown on Si, with excitations of 1, 16, 32, 79 and 334 kW·cm^{-2}. The dashed curves are Gaussian fitting

curves corresponding to the emission from the AlGaN layer and the GaN nanowire template, respectively.

In this model, we include the first-order and the higher-order nonradiative recombinations, as well as the bimolecular radiative recombination. Using the steady-state approximation, we have $G = R = An + Bn^2 + Cn^3$, where G is the excess carrier generation rate under optical excitation, R is the recombination rate, n is the carrier density; and A, B, and C are the first-order nonradiative recombination coefficient, the bimolecular radiative recombination coefficient, and the higher-order nonradiative recombination coefficient, respectively. Furthermore, expressing $I_{PL} = \gamma Bn^2$, where γ is a constant that includes the PL collection efficiency, injection efficiency, light extraction efficiency, and the active region volume, we have,

$$G = \frac{A}{\sqrt{B\gamma}}\sqrt{I_{PL}} + \frac{1}{\gamma}I_{PL} + \frac{C}{\sqrt{(B\gamma)^3}}\sqrt{(I_{PL})^3}. \quad (1)$$

Separately, G can be determined experimentally by

$$G = P_{\text{laser}}(1 - R_F)\alpha/(A_{\text{spot}}h\nu), \quad (2)$$

where P_{laser} is the peak optical power, R_F is Fresnel reflection at the sample surface, α is the absorption coefficient (25 μm^{-1}) of the sample, A_{spot} is the effective area of the laser pulse (300 μm × 300 μm) incident on the sample, and $h\nu$ is the photon energy (5.8 eV) of the laser. R_F was estimated to be around 7% using Fresnel's law, wherein the effective refractive index of the nanowire-air composite was determined by the Maxwell-Garnett equation. This R_F value is similar to the typically reported numbers from GaN-based nanowires, e.g., 4 % (Ref. 37). In addition, comparing the two samples,

the nanowire fill factor variation is small, which validates using the same R_F for both samples.

Using I_{PL} extracted from Fig. 2 under different excitation powers P_{laser} and Eq. (2), one can generate the G - I_{PL} dependence experimentally, which is further fitted to Eq. (1). This will allow one to determine A, B, C, and γ. It is noted, however, at this point, there are different sets of A, B, and C that can fit the experimental data with Eq. (1). To further determine A, B, and C, a separate evaluation of the recombination coefficient is required. In the previous studies, the B coefficient was fixed to 2.0×10^{-11} $cm^3\cdot s^{-1}$ to evaluate the lower boundary of IQE. [32,33,38] Here, following the similar idea, a B value of 2.0×10^{-11} $cm^3\cdot s^{-1}$ is used in our analysis. With this route, the carrier density n can be further calculated using $I_{PL} = \gamma Bn^2$, which further allows us to derive the carrier density dependent IQE via

$$IQE = Bn^2/(An + Bn^2 + Cn^3). \quad (3)$$

Figures 3(a) and 3(b) show the experimentally determined G versus I_{PL} in a linear scale, whereas the insets show the corresponding G versus I_{PL} in a logarithmic scale that manifest the nonlinearity of the G-I_{PL} dependence. The fitting curves using Eq. (1) are also shown, and it is seen that an excellent fitting can be obtained, which allows us to determine A and C with B fixed at 2.0×10^{-11} $cm^3\cdot s^{-1}$ and further allows us to calculate the carrier density dependent IQE.

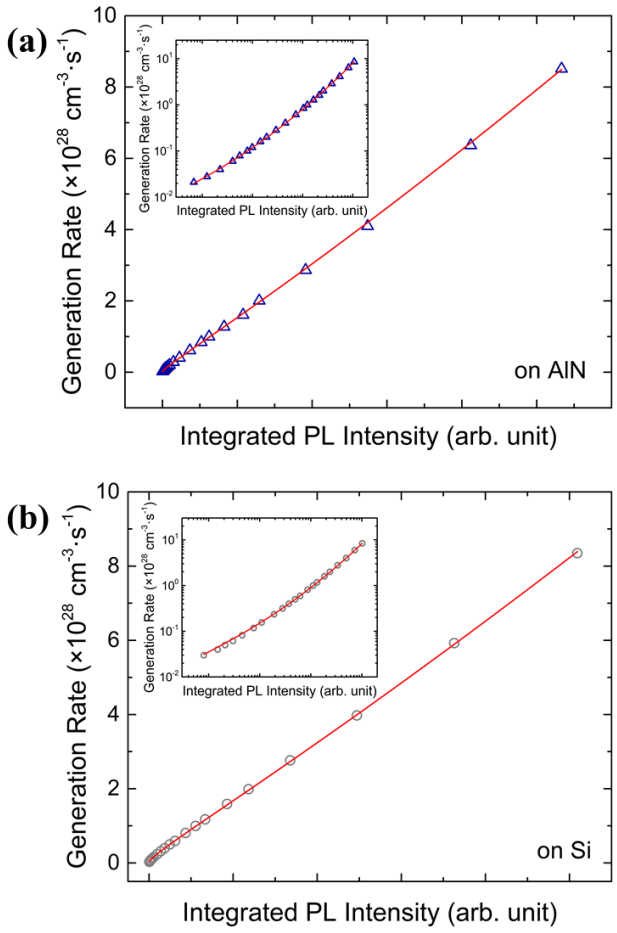

FIG. 3. (a) and (b) G vs I_{PL} for the AlGaN nanowire structures grown on the AlN buffer layer and on Si, respectively. The insets are G vs I_{PL} in a logarithmic scale. The solid curves are fitting curves according to Eq. (1).

The derived carrier density-dependent IQE is shown in Fig. 4. It is seen that, at a carrier density of 1×10^{18} cm^{-3}, the IQE for the AlGaN nanowire structures grown on the AlN buffer layer is improved (~14%) compared with the nanowire structures grown on Si directly (~10%). This is directly correlated to A coefficient of 1.19×10^{8} s^{-1} and 1.63×10^{8} s^{-1} for the nanowire structures grown on the AlN buffer layer and on Si, respectively. Moreover, the sample grown on the AlN buffer layer also shows an improved peak IQE. This improved optical quality could be attributed to the improved

nanowire vertical alignment and thus the reduced coalescence as suggested by the electron microscopy studies as presented earlier. In addition, the development of efficiency droop is seen from both samples at high carrier densities, correlating to non-negligible *C* coefficients of 1.31×10^{-31} $cm^6\cdot s^{-1}$ and 1.25×10^{-31} $cm^6\cdot s^{-1}$ for AlGaN nanowires grown on the AlN buffer and on Si, respectively.[39] It is noted, though, fixing the *B* coefficient may lead to an overestimate of the *C* coefficient.

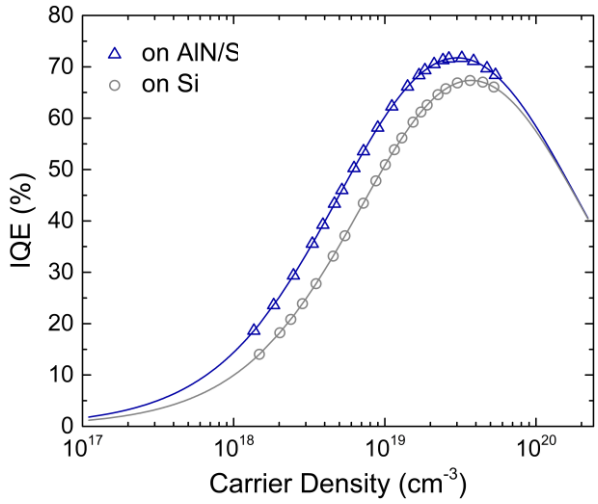

FIG. 4. Calculated IQE as a function of *n* for the AlGaN nanowire structures grown on the AlN buffer layer and on Si. The solid curves are the extrapolated curves based on the derived recombination coefficients.

As mentioned earlier, prior to this study, the IQE of AlGaN nanowire structures is often examined by the temperature-dependent PL by assuming the low-temperature IQE to be 100%, which is not necessarily a valid assumption. This study, on the other hand, provides a more thorough understanding of the carrier-density dependent IQE though analysing the recombination coefficients. Therefore, it allows the comparison between the AlGaN layer in the presented AlGaN nanowire structures and AlGaN

quantum wells. For the previously reported AlGaN quantum wells emitting in the wavelength range of 300 – 350 nm,[33] the typical range for *A* at room temperature is 3.5×10^{7} – 4.5×10^{8} s^{-1}, and the IQE at a carrier density of 1×10^{18} cm^{-3} is in the range of 5 – 40%. Therefore, it is seen that the room-temperature *A* coefficient and IQE of the AlGaN layer in the presented AlGaN nanowires (regardless on AlN buffer layer and on Si) are within the range of the previously reported values from AlGaN quantum wells.

In the end, we would like to discuss the limitation of our analysis. From Fig. 2, it is seen that the laser excitation contributes to emission from both the AlGaN segment and the GaN nanowire template. At high excitations, the GaN emission peak becomes non-negligible; and therefore, our approach tends to underestimate the IQE of the AlGaN layers at high excitations. However, due to the similar portion of the intensity of the GaN peak to the total emission intensity for both samples, our comparison between the two samples is still valid. Moreover, it is also noted that, as at low excitations, the intensity of the GaN peak is negligible compared with that of the AlGaN peak, our estimation of the IQE at low excitations is not affected by the GaN peak.

IV. SUMMARY AND CONCLUSIONS

In this work, we have provided a comparative study on the MBE growth and characterization of AlGaN/GaN nanowires on an AlN buffer layer on Si and on Si directly. A correlation between the structural property and optical quality for such nanowire structures is suggested. Specifically, for AlGaN nanowire structures grown

on the AlN buffer layer, owing to the improved nanowire vertical alignment and thus uniformity, an improved IQE is found, compared with the nanowire structures grown on Si directly. A further improvement can be obtained by surface passivation. The excellent structural and optical qualities, together with the possibility of doping AlN buffer layers to n-type, make such AlGaN nanowire structures, formed on an intermediate AlN buffer layer, an appealing route for semiconductor deep UV light emitters on Si.

ACKNOWLEDGMENTS

This work was supported under the Natural Sciences and Engineering Research Council of Canada (NSERC) RGPIN-2019-04726, NSERC DGECR-2019-00494, and McGill University.

Reference

[1]S. W. Eaton, A. Fu, A. B. Wong, C. Z. Ning and P. Yang, Nat. Rev. Mater. **1**, 16028 (2016).

[2]M. Kneissl, T. Y. Seong, J. Han and H. Amano, Nat. Photonics **13**, 233-244 (2019).

[3]F. Glas, Phys. Rev. B **74**, 121302 (2006).

[4]D. E. Perea, E. R. Hemesath, E. J. Schwalbach, J. L. Lensch-Falk, P. W. Voorhees and L. J. Lauhon, Nat. Nanotechnol. **4**, 315-319 (2009).

[5]S. Zhao, A. T. Connie, M. H. Dastjerdi, X. H. Kong, Q. Wang, M. Djavid, S. Sadaf, X. D. Liu, I. Shih, H. Guo and Z. Mi, Sci. Rep. **5**, 8332 (2015).

[6]Z. Fang, E. Robin, E. Rozas-Jimenez, A. Cros, F. Donatini, N. Mollard, J. Pernot and B. Daudin, Nano Lett. **15**, 6794-6801 (2015).

[7]S. Zhao, B. H. Le, D. P. Liu, X. D. Liu, M. G. Kibria, T. Szkopek, H. Guo and Z. Mi, Nano Lett. **13**, 5509-5513 (2013).

[8]H. Sun and X. Li, Phys. Status Solidi (A) **216**, 1800420 (2018).

[9]C. Zhao *et al.*, Prog. Quantum Electron. **61**, 1-31 (2018).

[10] J. Min *et al.*, J. Nanophotonics **12**, 043511 (2018).

[11]S. Zhao, J. Lu, X. Hai and X. Yin, Micromachines (Basel) **11**, 125 (2020).

[12]S. M. Sadaf, S. Zhao, Y. Wu, Y. H. Ra, X. Liu, S. Vanka and Z. Mi, Nano Lett. **17**, 1212-1218 (2017).

[13]S. Zhao, S. M. Sadaf, S. Vanka, Y. Wang, R. Rashid and Z. Mi, Appl. Phys. Lett. **109**, 201106 (2016).

[14]R. Songmuang, O. Landré and B. Daudin, Appl. Phys. Lett. **91**, 251902 (2007).

[15]T. Auzelle, B. Haas, A. Minj, C. Bougerol, J. L. Rouvière, A. Cros, J. Colchero and B. Daudin, J. Appl. Phys. **117** (2015).

[16]B. J. May, A. T. M. G. Sarwar and R. C. Myers, Appl. Phys. Lett. **108**, 141103 (2016).

[17]B. J. May, E. C. Hettiaratchy, C. Selcu, B. Wang, B. D. Esser, D. W. McComb and R. C. Myers, J. Vac. Sci. Technol. B **37**, 031212 (2019).

[18]H. Sun *et al.*, ACS Photonics **5**, 964-970 (2017).

[19]Y. Wu, Y. Wang, K. Sun and Z. Mi, J. Cryst. Growth **507**, 65-69 (2019).

[20]C. Zhao, T. K. Ng, N. Wei, A. Prabaswara, M. S. Alias, B. Janjua, C. Shen and B. S. Ooi, Nano Lett. **16**, 1056-1063 (2016).

[21]A. T. Sarwar, S. D. Carnevale, F. Yang, T. F. Kent, J. J. Jamison, D. W. McComb and R. C. Myers, Small **11**, 5402-5408 (2015).

[22]L. Largeau, E. Galopin, N. Gogneau, L. Travers, F. Glas and J.-C. Harmand, Cryst. Growth Des. **12**, 2724-2729 (2012).

[23]M. D. Brubaker, S. M. Duff, T. E. Harvey, P. T. Blanchard, A. Roshko, A. W. Sanders, N. A. Sanford and K. A. Bertness, Cryst. Growth Des. **16**, 596-604 (2015).

[24]M. D. Brubaker, I. Levin, A. V. Davydov, D. M. Rourke, N. A. Sanford, V. M. Bright and K. A. Bertness, J. Appl. Phys. **110**, 053506 (2011).

[25]K. A. Bertness, A. Roshko, L. M. Mansfield, T. E. Harvey and N. A. Sanford, J. Cryst. Growth **300**, 94-99 (2007).

[26]H. Sekiguchi, T. Nakazato, A. Kikuchi and K. Kishino, J. Cryst. Growth **300**, 259-262 (2007).

[27]S. Fernandez-Garrido, X. Kong, T. Gotschke, R. Calarco, L. Geelhaar, A. Trampert and O. Brandt, Nano Lett. **12**, 6119-6125 (2012).

[28]J. Ristić, E. Calleja, S. Fernández-Garrido, L. Cerutti, A. Trampert, U. Jahn and K. H. Ploog, J. Cryst. Growth **310**, 4035-4045 (2008).

[29]C. Himwas, M. den Hertog, L. S. Dang, E. Monroy and R. Songmuang, Appl. Phys. Lett. **105**, 241908 (2014).

[30]A. Pierret, C. Bougerol, S. Murcia-Mascaros, A. Cros, H. Renevier, B. Gayral and B. Daudin, Nanotechnology **24**, 115704 (2013).

[31]Y. Zhong, E. Berikaa, J. Lu, X. Yin, and S. Zhao, AIP Adv. 10, 025022 (2020).

[32]Z. Bryan, I. Bryan, J. Xie, S. Mita, Z. Sitar and R. Collazo, Appl. Phys. Lett. **106**,

142107 (2015).

[33]K. Ban, J. I. Yamamoto, K. Takeda, K. Ide, M. Iwaya, T. Takeuchi, S. Kamiyama, I. Akasaki and H. Amano, Appl. Phys. Express **4**, 052101 (2011).

[34]K. Yasutake, A. Takeuchi, H. Kakiuchi and K. Yoshii, J. Vac. Sci. Technol. A **16**, 2140-2147 (1998).

[35]S. Dasgupta, F. Wu, J. S. Speck and U. K. Mishra, Appl. Phys. Lett. **94**, 151906 (2009).

[36]F. Semond, B. Damilano, S. Vézian, N. Grandjean, M. Leroux and J. Massies, Appl. Phys. Lett. **75**, 82-84 (1999).

[37]W. Guo, M. Zhang, P. Bhattacharya and J. Heo, Nano Lett **11**, 1434-1438 (2011).

[38] Q. Dai *et al.*, Appl. Phys. Lett. **94**, 111109 (2009).

[39]J. Cho, E. F. Schubert and J. K. Kim, Laser Photonics Rev. **7**, 408-421 (2013).

5. Light Extraction Efficiency of AlGaN Nanowire Photonic Crystal Deep UV LEDs

In this chapter, an investigation of LEE of a complete AlGaN nanowire photonic crystal deep UV LED, considering a Si substrate and graphene electrode, is presented, being a guidance to the practical device design. The progress on using nanostructures to enhance the LEE of planar UV LEDs is also discussed.

5.1. Improvement of light extraction efficiency of UV LEDs with nanostructures

In general, the large amount of light being trapped inside the device structure, due to total internal reflection (TIR) at the semiconductor/air interface, is the main cause for the low LEE. In addition, for high Al content AlGaN deep UV LEDs, the unique optical polarization switching as mentioned earlier is another reason. To overcome the problems, different approaches have been applied to enhance the light extraction, such as surface roughening, substrate patterning, and exploiting photonic crystal structures.

Fig. 5 shows a comparison of LEE between a flip-chip (FC) LED and a FC LED with the top *n*-AlGaN layer textured.[36] For the untextured FC LED in Figs. 5(a) and (b), a maximum LEE of only ~1% is achieved for the TM-polarized emission at 280 nm. The LEE for the textured FC LED (Figs. 5(c) and (d)), in contrast, can be up to 45%, owning to light scattering.[36] Apart from the randomly textured surfaces, micro-structured arrays made of polymers, SiO_2 or TiO_2 have also been demonstrated.[53-57]

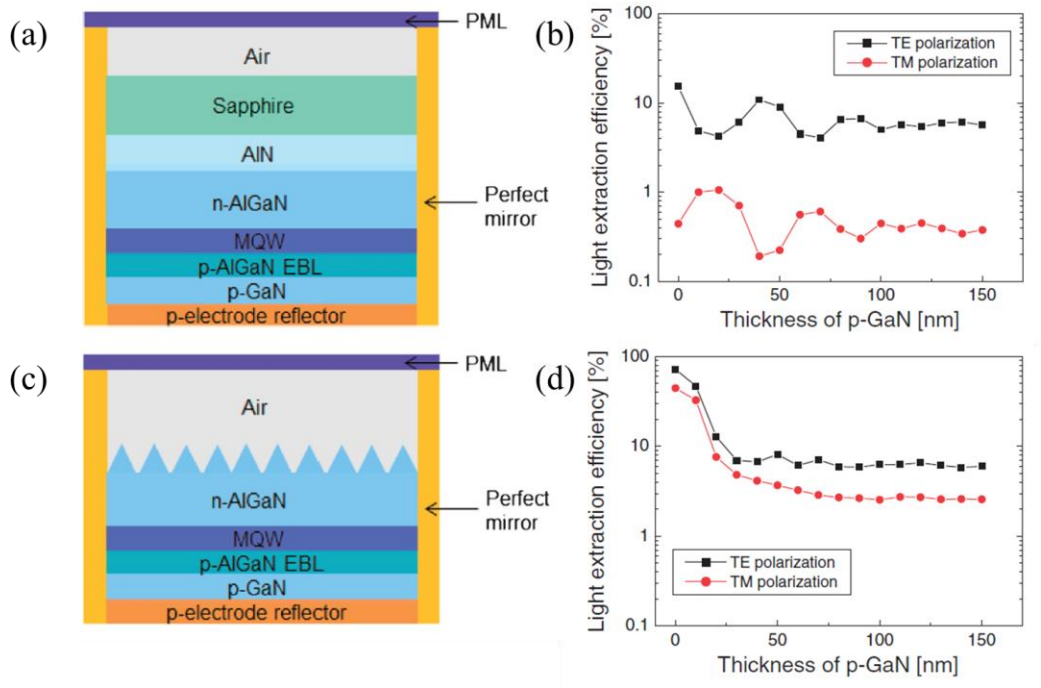

Fig. 5 (a) Schematic of simulation, and (b) simulated LEE vs. *p*-GaN thickness for FC LED emitting at 280 nm. (c) Schematic of simulation, and (d) simulated LEE vs. *p*-GaN thickness for FC LED structure with textured n-AlGaN layer.[36] © 2013 The Japan Society of Applied Physics.

Patterned sapphire substrates (PSS) have also been widely used to promote light extraction through light scattering.[58-61] The advantages of using PSS include less fabrication complexity and reduced TDDs.[62] The sapphire substrates can be etched to have various patterns as shown in Fig. 6. It is found that the morphology of the sapphire surface patterning not only affects TDDs, but also have an influence on the light extraction.[59-61] Figs. 6(a)-(c) show the SEM images of different-sized PSS patterns fabricated by the inductively coupled plasma (ICP) etching process. The detailed studies through TEM and simulation have revealed that TDDs show a decreasing trend with increasing the pattern size and fill factor (FF), while the LEE shows a decreasing trend.[59]

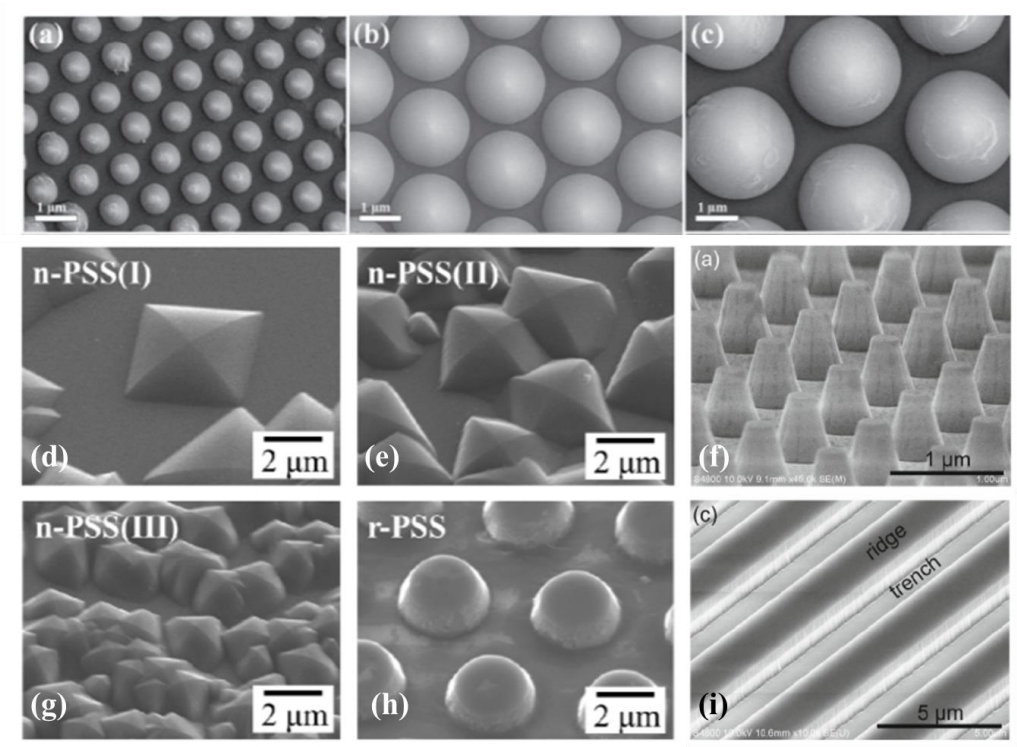

Fig. 6 (a)-(c) top-view SEM images of different-sized PSSs.[59] © 2017 The Japan Society of Applied Physics. (d)-(i) bird's eye-view SEM images of various PSS patterning.[60, 61]

Utilizing photonic crystals is another effective approach to improve LEE. In principle, light extraction can be enhanced in a photonic crystal via two routes: (1) Bragg diffraction, i.e., modes that satisfy $\boldsymbol{k}\pm\boldsymbol{G} < \boldsymbol{k_0}$ (where $\boldsymbol{G}$ is the reciprocal lattice vector of the photonic crystal, $\boldsymbol{k}$ and $\boldsymbol{k_0}$ are the in-plane wave vector in the semiconductor and in the air, respectively) become radiation modes, such that more light can be extracted into air.[35, 63, 64] (2) By letting the reduced frequency (a/λ) lie in the photonic crystal bandgap, the in-plane light propagation is prohibited, resulting in enhanced vertical propagation.[35, 65-68]

The effect of photonic crystals on the LEE relies on the design parameters such as lattices, spacings, geometries, and sizes. These factors define where the reduced

frequency situate and thus the mechanism of the LEE improvement. Photonic crystals can be introduced to LEDs by either adding a separate photonic crystal layer at the top (shown in Fig. 7(a)), or by arranging the nanowires in a way that resembles a photonic crystal (shown in Fig. 7(b)).[35, 64, 69, 70] With the use of photonic crystals, LEE in the range of 30-40% can be expected for TM-polarized emission wavelength of 240-260 nm, taking account the absorption of p-contact and metal contact.[35, 69]

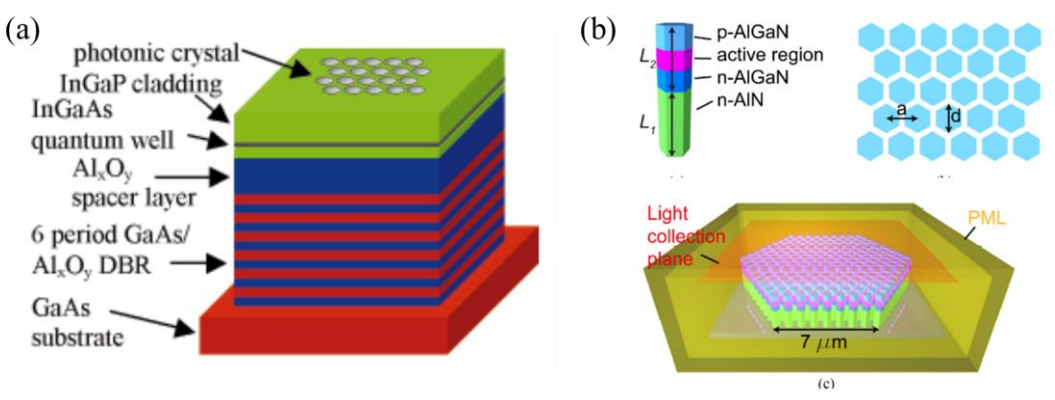

Fig. 7 (a) Schematic of a LED structure with a hexagonal photonic crystal layer on top. [64] (b) Schematic of an AlGaN nanowire photonic crystal LED structure.[69]

5.2. Manuscript

The following manuscript investigates the LEE of a practical AlGaN nanowire deep UV LED on Si arranged in different lattices, being a guidance for future device fabrication. The manuscript is formatted as the journal's submission template.

Light extraction efficiency of AlGaN nanowire deep ultraviolet light-emitting diodes on Si with different photonic structures

Jiaying Lu[†], Mohammad Fazel Vafadar[†] and Songrui Zhao[*]
McGill University, Department of Electrical and Computer Engineering, 3480 University Street, Montreal, Quebec, Canada, H3A0E9

Abstract. The low light extraction efficiency (LEE) stemming from the transverse-magnetic (TM) dominant emission is one of the major factors limiting the performance of AlGaN-based deep ultraviolet (UV) LEDs when the light emission wavelengths are close to 200 nm. These wavelengths, nonetheless, are pivotal to applications including sensing and sterilization, and are considered human safe. In this context, we investigate the LEE of AlGaN/AlN nanowire (NW) deep UV LED structures emitting at 225 nm, with a focus on the top-surface LEE by considering different NW arrangements, typical NW spacings and radii from AlGaN NWs grown by selective area epitaxy, the influence of Si on the LEE in comparison to an Al reflector, and graphene as the top electrode. Our results show that given the selected range of design parameters, the top-surface LEE for honeycomb, square, and hexagonal lattices can be up to around 42% for complete devices on Si with the graphene top electrode; and compared to using an Al reflector, the Si substrate does not reduce LEE considerably. In the end, the light extraction mechanism is discussed by simulating the 2-dimensional (2D) photonic crystal (PhC) band structures.

Keywords: AlGaN nanowires, deep ultraviolet, light-emitting diodes, light extraction efficiency, photonic crystal.

***** E-mail: songrui.zhao@mcgill.ca

1 Introduction

Aluminum gallium nitride (AlGaN) deep ultraviolet (UV) light-emitting diodes (LEDs) are promising to replace toxic mercury lamps for applications in water/air purification,

medical sensing, and sterilization.[1] In contrast to the indium gallium nitride (InGaN)-based near-UV LEDs which exhibit relatively high external quantum efficiencies (EQEs), the efficiency of AlGaN-based quantum well deep UV LEDs has remained low.[1, 2] Especially, as the light emission wavelengths approach to 200 nm, the EQE is only ~0.01% or less.[1] Nonetheless, these ultra-short emission wavelengths have been proven to be effective to inactivate pathogens, such as influenza viruses and coronaviruses, and more importantly, without doing any harm to human healthy tissues.[3, 4]

Such a low efficiency is limited not only by the material quality and the difficulty in the p-type doping, but also by the low light extraction efficiency (LEE). For AlGaN alloys, one major factor that limits the LEE is the optical polarization switching, i.e., as the Al content increases, the light emission from AlGaN alloys changes from the transverse-electric (TE) polarization to the transverse-magnetic (TM) polarization. This prohibits the light to escape from the top surface and results in extremely low LEE from top surface, e.g., less than 1% for the light emission at 210 nm.[5] This issue hinders the development of AlGaN-based surface-emitting deep UV LEDs which are more practically desirable compared to edge-emitting devices.

One-dimensional (1D) nanowire (NW) structures have received increasing attention due to several advantages such as better lattice strain accommodation owning to the large surface-to-bulk volume ratio, the reduced piezoelectric field, and better p-type

doping.[6, 7] Moreover, recent studies have shown that NW structures favor the TM-polarized light emission from the top surface.[8-12] For example, it has been shown experimentally that AlN NW LEDs emitting at 207 nm exhibit a top-surface dominant emission due to a strong light scattering effect.[13] Also, theoretical studies have further shown that by using tapered AlGaN NWs, more light can be coupled into the radiation modes, due to the break of the symmetry along the vertical direction.[8] It has also been shown that AlInN periodic NW arrays emitting at 300 nm can have a LEE of up to 60% from the top surface.[11]

Albeit the progress, there have been no studies on the large-area AlGaN NW deep UV LEDs emitting close to 200 nm, let alone the comparison of different lattices for the top-surface LEE at these short wavelengths. Furthermore, lattices other than hexagonal and square, e.g., honeycomb, have been barely reported for deep UV light emitting. A detailed comparison among different lattices could provide more insights into the design of future AlGaN NW deep UV LEDs at ultra-short wavelengths. Lastly, the existing theoretical studies mainly focus on transparent substrates and/or assume a 100% reflection. There are only limited theoretical studies on devices on Si substrates, in contrast with numerous experimental work on AlGaN NW deep UV LEDs on Si, e.g., Refs.[6,14,15] Understanding devices on Si will not only further improve the performance of devices on Si but also enable the IC industry process compatible, chip-on-board (COB) LEDs.

With these motivations, in this work, we examine the LEE of 225 nm emitting AlGaN/AlN NW deep UV LEDs on Si using the finite-difference time-domain (FDTD) method, with a focus on the top-surface LEE. Different Archimedes lattices, i.e., honeycomb, square, and hexagonal are considered. The NW diameter is in the range of 100-600 nm, and the edge-to-edge spacing is in the range of 10-80 nm. These diameter and spacing ranges are taken from the typical numbers of AlGaN NWs grown by selective area growth (SAG) with molecular beam epitaxy (MBE), which has demonstrated large-scale devices including both LEDs and lasers.[16, 17] Moreover, we further add a graphene layer as the top electrode, considering its excellent optical transparency in deep UV range as well as the excellent electrical conductivity and mechanical strength.[18, 19] As such, we evaluate complete LED devices, and hence our study could serve as a practical guide for the design of ultra-short-wavelength AlGaN NW deep UV LEDs on Si. It is found that such complete LED devices can provide a maximum top-surface LEE of around 42%, regardless of lattice structures. To further elucidate the mechanism of the top-surface LEE enhancement compared to conventional planar structures, the 2-dimensional (2D) photonic crystal (PhC) band structures for these lattices are investigated. It is found that with the design parameters for the highest top-surface LEE, all three lattices support radiation modes.

2 Methods

We used 3-dimensional (3D) FDTD simulation to calculate the light extraction efficiency of NW arrays. The LEE was defined as the ratio of the total extracted light power to the power emitted from the active region. In order to measure the light power, an electromagnetic field monitor was placed at the designated location which records the Poynting vector for each mesh cell. Integration of the Poynting vectors over the area of monitor returned the extracted power from a structure, as in Eq. (1).

$$Power(f) = \frac{1}{2}\int_{monitor} Re(\mathbf{P}(f)) \cdot d\mathbf{S} \quad (1)$$

For the photonic band structure calculation, we used 2D space and wave optics package in COMSOL Multiphysics.

3 Results and Discussions

The simulated structure is schematically shown in **Fig. 1(a)**. The structure is on Si substrate. For each individual NW, it consists of 10 nm n-GaN layer, 300 nm n-AlN layer, 60 nm $Al_{0.85}Ga_{0.15}N$ layer as the active region, 100 nm p-AlN layer, and 10 nm p-GaN layer. The bottom 10 nm GaN is necessary for the NW nucleation, whereas the top 10 nm GaN is for the low-resistivity p-type contact. The NWs are arranged in a honeycomb lattice, a square lattice, and a hexagonal lattice, respectively (**Figs. 1(b)-(d)**). The spacing and radius are in the range of 10-80 nm and 50-300 nm, respectively. It is noted that the spacing in this work refers to the edge-to-edge spacing between two adjacent NWs. The refractive indices of AlN and $Al_{0.85}Ga_{0.15}N$ are 2.67 and 2.7,

respectively. The absorption coefficients of the active region and GaN are assumed to be 1,000 cm^{-1} and 370,000 cm^{-1}, respectively. All the parameters are summarized in Table I.

Table 1 Parameters used for the simulation.

Parameters	Values
Refractive index of n/p-GaN	2.79
Refractive index of n/p-AlN	2.67
Refractive index of i-AlGaN	2.7
Absorption coefficient of n/p-GaN	370,000 cm^{-1}
Absorption coefficient of n/p-AlN	0
Absorption coefficient of i-AlGaN	1,000 cm^{-1}
Thickness of n-GaN	10 nm
Thickness of n-AlN	300 nm
Thickness of i-AlGaN	60 nm
Thickness of p-AlN	100 nm
Thickness of p-GaN	10 nm
Dipole type	TM mode
Temperature	300 K
Center wavelength	225 nm

In the FDTD simulation, we used 12 steep-angle perfect matched layers (PML) surrounding the simulated structure to annihilate all the incoming waves. A minimum

mesh step size of 0.25 nm was used. A dipole source emitting at 225 nm was placed at the center of the active region. In our implementation, the dipole was set to be TM polarized. The light output power was recorded by monitors placed both above and aside the structure. In this simulation, the total LEE referred to the ratio of the total extracted power from all surfaces to the total emitted power of the dipole source. The top-surface LEE referred to the ratio of the extracted power from the top surface to the total emitted power of the dipole source.

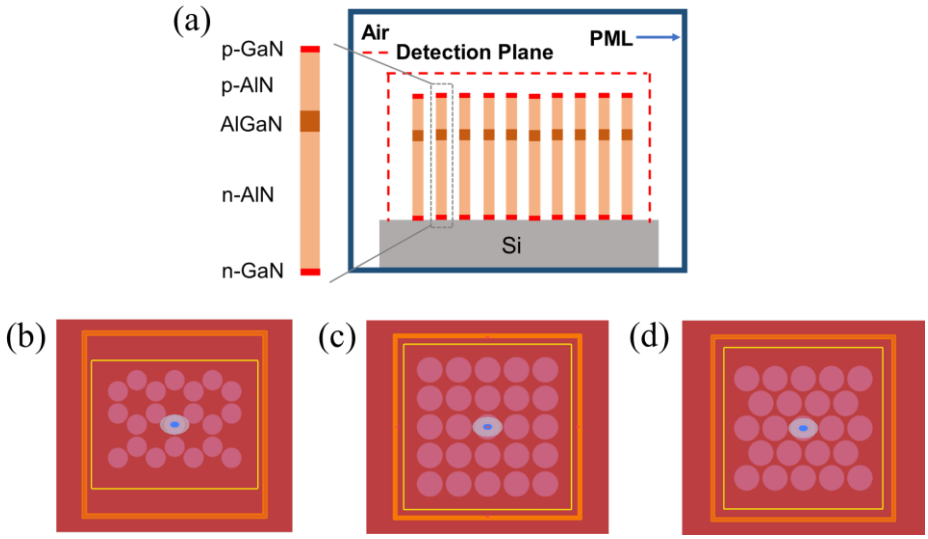

Fig. 1. (a) The simulated AlGaN NW deep UV LED device structure. (b)-(d) FDTD simulation setup for honeycomb, square and hexagonal NW array, respectively.

3.1 Investigation on the light extraction efficiency for different NW arrays

Figures 2 (a) and (b) show the contour plots of the LEE vs. the edge-to-edge spacing and radius for a honeycomb array. It is seen that the maximum total LEE is 66.6%, occurring at the spacing of around 50 nm and the radius of around 55 nm, whereas the top-surface LEE has a maximum of 42.2% at the spacing of around 70 nm and the

radius of around 80 nm, with a total LEE of 53.7%. In addition to the absolute LEEs, we introduce the top/total LEE ratio as a measure of the competence of the structure in extracting the light from the top surface. A higher ratio indicates that a greater portion of the light is extracted from the top surface. For the honeycomb lattice, the top/total LEE ratio is 0.786 when the top-surface LEE is at the maximum. This suggests that with the parameters giving a maximum top-surface LEE, the majority of the light is forced to propagate along the vertical direction, leaving little light to escape from the lateral surface.

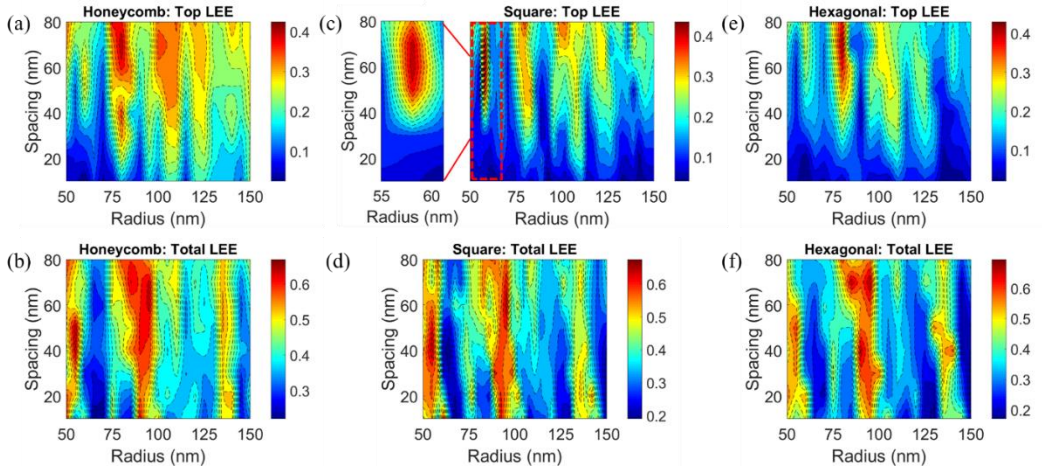

Fig. 2. Contour plots of (a) the top-surface LEE and (b) the total LEE vs. the NW radius and the edge-to-edge spacing for the honeycomb lattice, respectively. (c) the top-surface LEE and (d) the total LEE vs. the NW radius and the edge-to-edge spacing for the square lattice, respectively. (e) the top-surface LEE and (f) the total LEE vs. the NW radius and the edge-to-edge spacing for the hexagonal lattice, respectively.

We have further examined the LEEs for the square lattice and hexagonal lattice. For the square lattice (**Figs.** 2(c) and 2(d)), the top-surface LEE has a maximum of 43.3% at the radius of around 58 nm and spacing of around 60 nm, with a total LEE of 52.0%.

For the hexagonal lattice (**Figs. 2**(e) and 2(f)), the maximum top-surface LEE is 42.9%, at the radius of around 80 nm and the spacing of around 70 nm, with a total LEE of 49.8%. The corresponding top/total LEE ratios are 0.833 and 0.861 for the square lattice and hexagonal lattice, respectively. Comparing the three NW arrays, they can provide similarly high top-surface LEEs with the respective optimized design parameters. The underlying mechanism is to be discussed in detail in a later section. It is further noted that the hexagonal lattice demonstrates the best competence of extracting the light from the top surface, evident from the highest top/total LEE ratio.

It is also noted that only the results for AlGaN NW radius below 150 nm are shown here, as the top-surface LEE drops drastically down to a single-digit number once the NW radius is above ~150 nm, regardless of the choice of the NW edge-to-edge spacing, reflecting the significant impact of the NW radius on the light extraction. This can be understood that thick NWs have reduced surface-to-bulk volume ratios, and thus more light is trapped in the NWs due to the total internal reflection (TIR) at the semiconductor-air interface.[8, 20] Furthermore, at moderately small radii, e.g., ~80 nm, the top-surface LEE increases with increasing the edge-to-edge spacing, owning to the formation of coupled modes in the NWs.[10, 20] Therefore, from the perspective of extracting the TM-polarized light from the top surface, it is more favorable to use small-radius NWs with relatively large spacings. In addition, the periodic fluctuation of the top-surface LEE and the total LEE can be observed for all the lattices, i.e., at certain nanowire radii, there present LEE minima regardless of the choice of the nanowire

spacing. These LEE minima are associated with the formation of resonant modes in nanowire arrays.[21,22]

Based on the optimized parameters for the maximum top-surface LEEs, **Fig. 3** shows the comparison of the electric field intensity distribution in a logarithmic scale of the NW structures in a cross-sectional view. It is seen that for all the three lattices, strong radiation is present at the top surface, with little guided modes, consistent with the large top/total LEE ratios obtained from the three lattices.

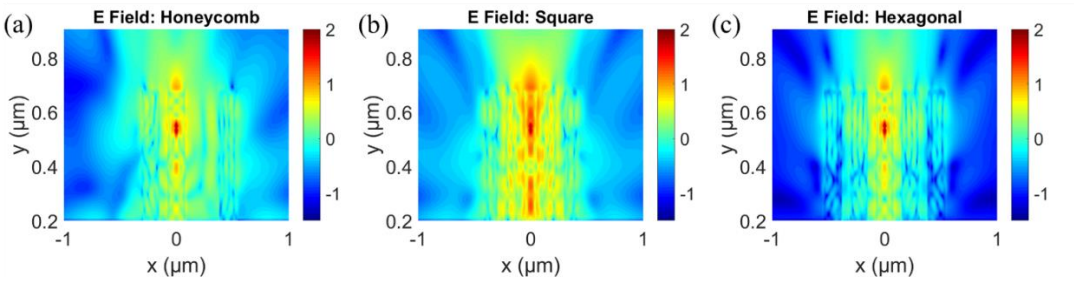

Fig. 3. Cross-sectional view of the TM-polarized electric field intensity distribution for AlGaN NWs arranged in (a) honeycomb lattice, (b) square lattice, and (c) hexagonal lattice.

We have further investigated the far-field radiation patterns of the AlGaN NWs with the parameters giving the maximum top-surface LEEs for different lattices. As shown in **Fig. 4**, the square lattice, among all the lattices, exhibits the highest far-field intensity, followed by honeycomb and hexagonal. It is also noticed that for the honeycomb lattice (Fig. 4(a)), the far-field intensity distribution pattern is less symmetric, while the square array presents a square ring pattern (**Fig. 4**(b)) and the hexagonal array shows a hexagonal symmetry (**Fig. 4** (c)). This difference can be attributed to the different NW

arrays that affect light scattering and thus the far-field radiation patterns.[23] The zenith angles (θ) of the far-field radiations are 40°, 45°, and 50° for honeycomb, square and hexagonal lattices, respectively, within the range of typical PhC LEDs.[23-25]

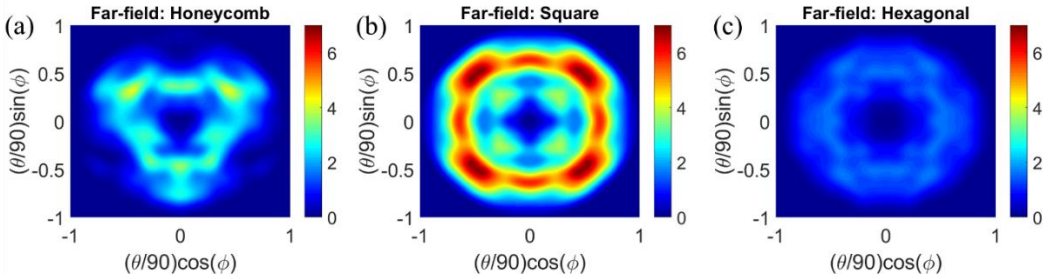

Fig.4. Far-field intensity distribution of AlGaN NWs in (a) honeycomb lattice, (b) square lattice, and (c) hexagonal lattice.

3.2 Evaluation of the Si substrate on the LEE

For the previous limited theoretical studies on AlGaN NW UV LEDs on Si, the role of Si on the LEE is not explicitly discussed. As such, here we study the effects of the Si substrate on both the top-surface and total LEEs in comparison with an Al reflector, with all the rest of the device structure being the same. Moreover, we further evaluate the difference in the LEE as a function of the GaN layer thickness.

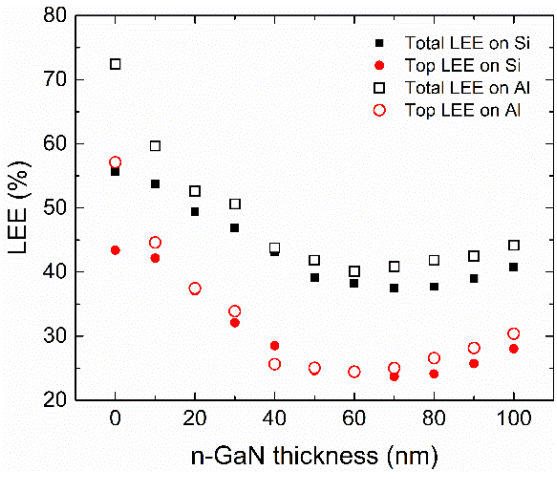

Fig.5. Variation of the total LEE and the top-surface LEE vs. the thickness of the n-

GaN layer for the AlGaN NW honeycomb array on Si (solid symbols) and on Al (open symbols), respectively.

Figure 5 shows a comparison of LEEs vs. the n-GaN thickness for AlGaN NW LEDs arranged in a honeycomb lattice on the Si substrate (solid symbols) and on an Al reflector (open symbols), respectively. The NW spacing and radius are fixed at 70 nm and 80 nm, respectively, whereas the n-GaN thickness is varying from 0 to 100 nm. Damped oscillations are seen as the GaN layer thickness increases, which is a typical behavior of the influence of the GaN layer thickness on the LEE.[26] Moreover, it is seen that compared to the Al reflector, the Si substrate does not reduce the LEE severely, which is in particular the case when the GaN layer is present.

This can be explained by that, although Si has a very high absorption coefficient at 225 nm (on the order of 10^6 cm^{-1}), the light is mostly reflected rather than absorbed, with a reflectivity of ~70%, due to the extremely short penetration depth.[27, 28] Separate studies on thin-film LEDs on Si substrates have shown an improved LEE due to the high reflectivity and the enhanced Fabry-Perot cavity effects at the GaN/Si interface.[27, 29]

So far, we have not considered the graphene top electrode. With graphene as the electrode added the LED structure top surface (**Fig. 1** (a)) and the rest being the same, the top-surface LEEs for honeycomb, square, and hexagonal lattices are up to 41.8%, 42.5%, and 42.3%, respectively.

3.3 Discussion on the light extraction mechanism

In principle, compared to planar structures, the light extraction can be enhanced in a PhC via two routes: (1) Bragg diffraction, i.e., the periodic PhC folds the guided modes at the Brillouin zone (BZ) boundary, allowing those that satisfy $\mathbf{k}\pm\mathbf{G} < \mathbf{k_0}$ (where **G** is the reciprocal lattice vector of the PhC, $\mathbf{k_0}$ is the in-plane wavevector in air, and **k** is the in-plane wavevector of the emitted light propagating in the medium) to become the radiation modes, such that more light can be extracted into the air.[8, 30, 31] (2) Setting the reduced frequency within the PhC bandgap, such that the in-plane light propagation is prohibited, resulting in the enhanced vertical light propagation.[8, 32, 33]

Here, in order to elucidate the mechanism, we further calculated the respective PhC band structures using COMSOL Multiphysics. In this simulation, eigenfrequency study and *k*-vector sweep across the irreducible Brillouin zone were performed to compute the bands. The unit cells for calculating the PhC band structures are shown in **Figs. 6** (a)-(c) wherein the radius (*R*), the edge-to-edge spacing (*S*), and the lattice constant (*a*) are annotated. It is noted that changing these parameters will not only change the band structures, but also shift the reduced frequency.

Figures 6 (d)-(f) show the 2D PhC band structures of the honeycomb, square, and hexagonal lattices, respectively. The light line, which is defined as $\omega = c|\boldsymbol{k_0}|$, is shown by the solid black line. Modes below the light line are guided and suffer from the TIR at the semiconductor/air interface, whereas the modes above the light line correspond to the radiation modes that can escape from the top surface. The red dashed line

represents the reduced frequency, i.e., a/λ. It is seen that for all three PhC structures, the reduced frequencies are located above the light line, so the modes are radiation modes, leading to the high top-surface LEEs compared to conventional planar AlGaN structures emitting in this wavelength range. It is also noted that compared to the other two lattices, the reduced frequency of honeycomb lattice is located very high above the light line, suggesting a wider range of the lattice constant *a* that can support the radiation modes.

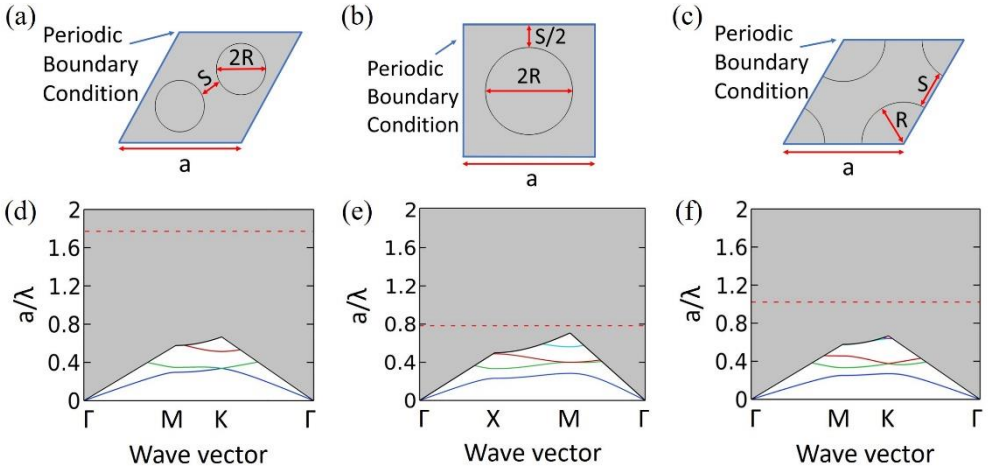

Fig.6. (a)-(c) COMSOL setup for honeycomb, square, and hexagonal NW array, respectively. The unit cell is outlined by blue quadrangle. (d)-(f) The 2D PhC band structures for the honeycomb lattice, square lattice, and hexagonal lattice based on the optimized design parameters for the best top-surface LEE.

4 Conclusion

In conclusion, we have simulated the LEEs of AlGaN NW deep UV LEDs on Si with different NW arrangements. The boundary conditions for NW radius and spacing in our

simulation are set by the typical values from AlGaN NWs grown by SAG using MBE. In addition, graphene is considered as the top electrode. For such complete LED devices emitting at 225 nm, the top-surface LEE up to 42% is derived, regardless of the NW arrangement (i.e., honeycomb, square, or hexagonal lattices). Moreover, compared with Al reflector, the use of Si does not severely reduce the top-surface LEE. We have further calculated the PhC band structures of these lattices, which reveals that the reduced frequencies for all the three lattices sit above the light line, explaining a similar maximum top-surface LEE. Nonetheless, comparing amongst the three lattices, the hexagonal lattice has the highest top/total LEE ratio, suggesting that the hexagonal lattice is more competent in extracting the light from the top surface.

Disclosures

The authors declare no conflicts of interest.

Author Contribution

[†]J. Lu and M. Vafadar contribute equally to this work.

Acknowledgements

This work is supported under Natural Sciences and Engineering Research Council of Canada (NSERC) and Fonds de Recherche du Quebec – Nature et Technologies (FRQNT).

Reference

1. M. Kneissl et al., "The emergence and prospects of deep-ultraviolet light-emitting diode technologies," *Nat. Photonics* **13**(4), 233-244 (2019).
2. T. Takano et al., "Deep-ultraviolet light-emitting diodes with external quantum efficiency higher than 20% at 275 nm achieved by improving light-extraction efficiency," *Appl. Phys. Express* **10**(3), 031002 (2017).
3. M. Buonanno, D. Welch, and I. Shuryak, "Far-UVC light (222 nm) efficiently and safely inactivates airborne human coronaviruses.," *Sci. Rep.* **10**, 10285 (2020).
4. D. Welch et al. "Far-UVC light applications: sterilization of MRSA on a surface and inactivation of aerosolized influenza virus," in *Light-Based Diagnosis and Treatment of Infectious Diseases, International Society for Optics and Photonics*, p 104791D (2018).
5. Y. Taniyasu, and M. Kasu, "Surface 210 nm light emission from an AlN p–n junction light-emitting diode enhanced by A-plane growth orientation," *Appl. Phys. Lett.* **96**(22), 221110 (2010).
6. J. W. Min et al., "Unleashing the potential of molecular beam epitaxy grown AlGaN-based ultraviolet-spectrum nanowires devices," *J. Nanophotonics* **12**(4), 043511 (2018).
7. S. Zhao et al., "AlGaN Nanowires for Ultraviolet Light-Emitting: Recent Progress, Challenges, and Prospects," *Micromachines* **11**(2), 125 (2020).
8. R. Lin et al., "Tapering-induced enhancement of light extraction efficiency of nanowire deep ultraviolet LED by theoretical simulations," *Photonics Res.* **6**(5), (2018).
9. P. Du, and Z. Cheng, "Enhancing Light Extraction Efficiency of Vertical Emission of AlGaN Nanowire Light Emitting Diodes With Photonic Crystal," *IEEE*

Photonics J. **11**(3), 1-9 (2019).

10. P. Du et al., "Enhancing the light extraction efficiency of AlGaN LED with nanowire photonic crystal and graphene transparent electrode," *Superlattices and Microst.* **133**, 106216 (2019).
11. B. Jain et al., "Enhancing the light extraction efficiency of AlInN nanowire ultraviolet light-emitting diodes with photonic crystal structures," *Opt. Express* **28**(15), 22908-22918 (2020).
12. L. Feng et al., "Effect of photonic crystals on the light extraction of GaN-based LED for different polarization modes of spontaneous radiation," *Results Phys.* **15**, 102632 (2019).
13. S. Zhao, M. Djavid, and Z. Mi, "Surface Emitting, High Efficiency Near-Vacuum Ultraviolet Light Source with Aluminum Nitride Nanowires Monolithically Grown on Silicon," *Nano Lett.* **15**(10), 7006-9 (2015).
14. S. Zhao et al., "Aluminum nitride nanowire light emitting diodes: Breaking the fundamental bottleneck of deep ultraviolet light sources," *Sci. Rep.* **5**, 8332 (2015).
15. S. Sadaf et al., "An AlGaN core–shell tunnel junction nanowire light-emitting diode operating in the ultraviolet-C band," *Nano Lett.* **17**(2), 1212-1218 (2017).
16. X. Liu et al., "Selective area epitaxy of AlGaN nanowire arrays across nearly the entire compositional range for deep ultraviolet photonics," *Opt. Express* **25**(24), 30494-30502 (2017).
17. B. Le et al., "An electrically injected AlGaN nanowire defect-free photonic crystal ultraviolet laser," *Opt. Express* **27**(4), 5843-5850 (2019).
18. F. Bonaccorso et al., "Graphene photonics and optoelectronics," *Nat. Photonics* **4**(9), 611 (2010).
19. M. Pumera, "Graphene-based nanomaterials and their electrochemistry," *Chem. Soc.*

Rev. **39**(11), 4146-4157 (2010).

20. M. Djavid, and Z. Mi, "Enhancing the light extraction efficiency of AlGaN deep ultraviolet light emitting diodes by using nanowire structures," *Appl. Phys. Lett.* **108**(5), 051102 (2016).
21. H. Y. Ryu, "Large enhancement of light extraction efficiency in AlGaN-based nanorod ultraviolet light-emitting diode structures," *Nanoscale Res. Lett.* **9**(1), 1-7 (2014).
22. Y. K. Ooi, C. Liu, and J. Zhang, "Analysis of Polarization-Dependent Light Extraction and Effect of Passivation Layer for 230-nm AlGaN Nanowire Light-Emitting Diodes," *IEEE Photonics J.* **9**(4), 1-12 (2017).
23. P. Zhu, andN. Tansu, "Effect of packing density and packing geometry on light extraction of III-nitride light-emitting diodes with microsphere arrays," *Photonics Res.* **3**(4), 184-191 (2015).
24. Y. K. Ooi, and J. Zhang, "Light extraction efficiency analysis of flip-chip ultraviolet light-emitting diodes with patterned sapphire substrate," *IEEE Photonics J.* **10**(4), 1-13 (2018).
25. Q. Jiao et al., "The effects of nanocavity and photonic crystal in InGaN/GaN nanorod LED arrays," *Nanoscale Res. Lett.* **11**(1), 340 (2016).
26. H. Y. Ryu et al., "Investigation of Light Extraction Efficiency in AlGaN Deep-Ultraviolet Light-Emitting Diodes," *Appl. Phys. Express* **6**(6), 062101 (2013).
27. D. Liu et al., "226 nm AlGaN/AlN UV LEDs using p-type Si for hole injection and UV reflection," *Appl. Phys. Lett.* **113**(1), 011111 (2018).
28. M. A. Green, "Self-consistent optical parameters of intrinsic silicon at 300K including temperature coefficients," *Sol. Energy Mater. Sol. Cells* **92**(11), 1305-1310 (2008).

29. S. Tripathy et al., "Light extraction from GaN-based LED structures on silicon-on-insulator substrates," *Phys. Status Solidi C* **7**(1), 88-91 (2010).
30. H. Ichikawa, and T. Baba, "Efficiency enhancement in a light-emitting diode with a two-dimensional surface grating photonic crystal," *Appl. Phys. Lett.* **84**(4), 457-459 (2004).
31. A. A. Erchak et al., "Enhanced coupling to vertical radiation using a two-dimensional photonic crystal in a semiconductor light-emitting diode," *Appl. Phys. Lett.* **78**(5), 563-565 (2001).
32. S. Fan, P. R. Villeneuve, and J. D. Joannopoulos, "Rate-Equation Analysis of Output Efficiency and Modulation Rate of Photonic-Crystal Light-Emitting Diodes," *IEEE J. Quantum Electron.* **36**, 1123-1130 (2000).
33. S. Fan, P. R. Villeneuve, and J. D. Joannopoulos, "High Extraction Efficiency of Spontaneous Emission from Slabs of Photonic Crystals," *Phys. Rev. Lett.* **78**(17), 3295 (1997).

6. Conclusion and Future Work

This thesis describes a body of work about studying the optical quality of AlGaN nanowires as the Al content and optical excitation change, as well as investigating the LEE of AlGaN nanowire deep UV LED with different photonic crystal structures. These studies are carried out with a ultimate goal of improving the EQE of AlGaN nanowire deep UV LEDs.

We have shown that a thin AlN layer is beneficial for the structural and optical qualities of AlGaN nanowires; however, electrically injected devices are yet to be studied. Future work includes p-/n-doping, heterostructure design, surface passivation, and forming a low-resistance ohmic p-/n-contact with doped AlGaN layers to make ensemble LED devices.

Furthermore, although the present study unveils the excitation and Al content dependent IQE, the Al content is only the in range of 22 – 54 mol%, and it is clear of great interest to examine the IQE behavior with even higher Al contents. Moreover, although the efficiency droop is seen from samples in the present study, limited by experiments, a conclusive droop mechanism cannot be reached. Further unveiling the droop mechanism is certainly worth studying in the future. In this regard, a wider Al content range, with even higher Al contents, is definitely beneficial to have a better understanding of the droop behavior in AlGaN nanowires.

It is further noted that, in the present study, to estimate IQE at low excitations, a theoretical radiative recombination B coefficient from bulk AlGaN is used. However, the B values in nanowires could be different from theoretical bulk values. It is thus of great interest to investigate the B coefficient in AlGaN nanowires, which not only gives a better understanding of the fundamental optical properties of AlGaN nanowires, but

also improves the estimation of the IQE at low excitations. This can be done, for example, by time-resolved photoluminescence (TRPL) or light-induced transient grating (LITG) technique.[71, 72]

Lastly, in the present study, it is shown that by using AlGaN nanowire photonic crystal structures, the LEE can be enhanced drastically compared to planar counterparts at the wavelength of 225 nm. Nonetheless, the effects of defects and nanowire geometry on the light extraction require further study. This will not only provide a holistic view of AlGaN deep UV nanowire LED design with efficient light extraction, but may also shine light on the design of AlGaN nanowire deep UV lasers.

Reference

[1] M. Kneissl, T.-Y. Seong, J. Han, and H. J. N. P. Amano, "The emergence and prospects of deep-ultraviolet light-emitting diode technologies," *Nature Photonics,* vol. 13, no. 4, pp. 233-244, 2019.

[2] T. Nishida and N. J. p. s. s. Kobayashi, "346 nm Emission from AlGaN Multi-Quantum-Well Light Emitting Diode," *Physica Status Solidi (A),* vol. 176, no. 1, pp. 45-48, 1999.

[3] T. Mukai, D. Morita, and S. J. J. o. C. G. Nakamura, "High-power UV InGaN/AlGaN double-heterostructure LEDs," *Journal of Crystal Growth,* vol. 189, pp. 778-781, 1998.

[4] H. Hirayama, *Recent progress in AlGaN deep-UV LEDs*. InTech, 2018.

[5] J.-W. Min *et al.*, "Unleashing the potential of molecular beam epitaxy grown AlGaN-based ultraviolet-spectrum nanowires devices," *Journal of Nanophotonics,* vol. 12, no. 4, p. 043511, 2018.

[6] H.-M. Wang, J.-P. Zhang, C.-Q. Chen, Q. Fareed, J.-W. Yang, and M. A. Khan, "AlN/AlGaN superlattices as dislocation filter for low-threading-dislocation thick AlGaN layers on sapphire," *Applied Physics Letters,* vol. 81, no. 4, pp. 604-606, 2002.

[7] H. Hirayama *et al.*, "Milliwatt power 270 nm-band AlGaN deep-UV LEDs fabricated on ELO-AlN templates," *Physica Status Solidi C,* vol. 6, no. S2 2, pp. S474-S477, 2009.

[8] S. Zhao *et al.*, "Aluminum nitride nanowire light emitting diodes: Breaking the fundamental bottleneck of deep ultraviolet light sources," *Scientific Reports,* vol. 5, p. 8332, Feb 16 2015.

[9] Y. Zhong, E. Berikaa, J. Lu, X. Yin, and S. Zhao, "Molecular beam epitaxial growth and optical characterization of AlGaN nanowires with reduced substrate temperature," *AIP Advances,* vol. 10, no. 2, p. 025022, 2020.

[10] H. Sun *et al.*, "Graded-Index Separate Confinement Heterostructure AlGaN Nanowires: Toward Ultraviolet Laser Diodes Implementation," *ACS Photonics,* vol. 5, no. 8, pp. 3305-3314, 2018.

[11] H. Yu *et al.*, "Enhanced performance of an AlGaN-based deep-ultraviolet LED having graded quantum well structure," *IEEE Photonics Journal,* vol. 11, no. 4, pp. 1-6, 2019.

[12] M. Jo, N. Maeda, and H. Hirayama, "Enhanced light extraction in 260 nm light-emitting diode with a highly transparent p-AlGaN layer," *Applied Physics Express,* vol. 9, no. 1, 2016.

[13] N. Maeda, M. Jo, and H. Hirayama, "Improving the Light-Extraction Efficiency of AlGaN DUV-LEDs by Using a Superlattice Hole Spreading Layer and an Al Reflector," *Physica Status Solidi (A),* vol. 215, no. 8, 2018.

[14] S. Zhao, J. Lu, X. Hai, and X. Yin, "AlGaN Nanowires for Ultraviolet Light-Emitting: Recent Progress, Challenges, and Prospects," *Micromachines,* vol. 11, no. 2, p. 125, 2020.

[15] Z. Fang *et al.*, "Si donor incorporation in GaN nanowires," *Nano Letters,* vol. 15, no. 10, pp. 6794-6801, 2015.

[16] N. H. Tran, B. H. Le, S. Zhao, and Z. Mi, "On the mechanism of highly efficient p-type conduction of Mg-doped ultra-wide-bandgap AlN nanostructures," *Applied Physics Letters,* vol. 110, no. 3, p. 032102, 2017.

[17] C. Zhao *et al.*, "Facile formation of high-quality InGaN/GaN quantum-disks-in-nanowires on bulk-metal substrates for high-power light-emitters," *Nano*

Letters, vol. 16, no. 2, pp. 1056-1063, 2016.

[18] A. G. Sarwar *et al.*, "Semiconductor nanowire light-emitting diodes grown on metal: a direction toward large-scale fabrication of nanowire devices," *Small,* vol. 11, no. 40, pp. 5402-5408, 2015.

[19] B. J. May, A. G. Sarwar, and R. C. Myers, "Nanowire LEDs grown directly on flexible metal foil," *Applied Physics Letters,* vol. 108, no. 14, p. 141103, 2016.

[20] J.-I. Shim and D.-S. Shin, "Measuring the internal quantum efficiency of light-emitting diodes: towards accurate and reliable room-temperature characterization," *Nanophotonics,* vol. 7, no. 10, pp. 1601-1615, 2018.

[21] Y. H. Ra, S. Kang, and C. R. Lee, "Ultraviolet Light-Emitting Diode Using Nonpolar AlGaN Core–Shell Nanowire Heterostructures," *Advanced Optical Materials,* vol. 6, no. 14, p. 1701391, 2018.

[22] S. Zhao, S. Sadaf, S. Vanka, Y. Wang, R. Rashid, and Z. Mi, "Sub-milliwatt AlGaN nanowire tunnel junction deep ultraviolet light emitting diodes on silicon operating at 242 nm," *Applied Physics Letters,* vol. 109, no. 20, p. 201106, 2016.

[23] X. Hai, R. Rashid, S. Sadaf, Z. Mi, and S. Zhao, "Effect of low hole mobility on the efficiency droop of AlGaN nanowire deep ultraviolet light emitting diodes," *Applied Physics Letters,* vol. 114, no. 10, p. 101104, 2019.

[24] S. Sadaf *et al.*, "An AlGaN core–shell tunnel junction nanowire light-emitting diode operating in the ultraviolet-C band," *Nano Letters,* vol. 17, no. 2, pp. 1212-1218, 2017.

[25] Y. Wu, Y. Wang, K. Sun, and Z. Mi, "Molecular beam epitaxy and characterization of AlGaN nanowire ultraviolet light emitting diodes on Al coated Si (0 0 1) substrate," *Journal of Crystal Growth,* vol. 507, pp. 65-69,

2019.

[26] A. G. Sarwar, B. J. May, J. I. Deitz, T. J. Grassman, D. W. McComb, and R. C. Myers, "Tunnel junction enhanced nanowire ultraviolet light emitting diodes," *Applied Physics Letters,* vol. 107, no. 10, p. 101103, 2015.

[27] X. Luo *et al.*, "Coaxial semipolar InGaN/GaN microwire array LED with substantially suppressed efficiency droop," *Journal of Luminescence,* vol. 221, p. 117014, 2020.

[28] S. D. Carnevale *et al.*, "Graded nanowire ultraviolet LEDs by polarization engineering," in *Nanoepitaxy: Materials and Devices IV*, 2012, vol. 8467, p. 84670L: International Society for Optics and Photonics.

[29] N. Guan *et al.*, "Flexible white light emitting diodes based on nitride nanowires and nanophosphors," *ACS Photonics,* vol. 3, no. 4, pp. 597-603, 2016.

[30] I. M. Høiaas *et al.*, "GaN/AlGaN Nanocolumn ultraviolet light-emitting diode using double-layer graphene as substrate and transparent electrode," *Nano Letters,* vol. 19, no. 3, pp. 1649-1658, 2019.

[31] M. Nami *et al.*, "Carrier dynamics and electro-optical characterization of high-performance GaN/InGaN core-shell nanowire light-emitting diodes," *Scientific Reports,* vol. 8, no. 1, pp. 1-11, 2018.

[32] Y. Taniyasu and M. Kasu, "Surface 210 nm light emission from an AlN p–n junction light-emitting diode enhanced by A-plane growth orientation," *Applied Physics Letters,* vol. 96, no. 22, p. 221110, 2010.

[33] Y. K. Ooi, C. Liu, and J. Zhang, "Analysis of Polarization-Dependent Light Extraction and Effect of Passivation Layer for 230-nm AlGaN Nanowire Light-Emitting Diodes," *IEEE Photonics Journal,* vol. 9, no. 4, pp. 1-12, 2017.

[34] X. Liu *et al.*, "Selective area epitaxy of AlGaN nanowire arrays across nearly

the entire compositional range for deep ultraviolet photonics," *Optics Express,* vol. 25, no. 24, pp. 30494-30502, 2017.

[35] R. Lin *et al.*, "Tapering-induced enhancement of light extraction efficiency of nanowire deep ultraviolet LED by theoretical simulations," *Photonics Research,* vol. 6, no. 5, 2018.

[36] H.-Y. Ryu, I.-G. Choi, H.-S. Choi, and J.-I. Shim, "Investigation of Light Extraction Efficiency in AlGaN Deep-Ultraviolet Light-Emitting Diodes," *Applied Physics Express,* vol. 6, no. 6, p. 062101, 2013.

[37] C. Zhao *et al.*, "III-nitride nanowires on unconventional substrates: From materials to optoelectronic device applications," *Progress in Quantum Electronics,* vol. 61, pp. 1-31, 2018.

[38] R. Jiang and X. Meng, "The characterization of AlGaN nanowires prepared via chemical vapor deposition," *Journal of Materials Science: Materials in Electronics,* vol. 30, no. 17, pp. 16266-16274, 2019.

[39] L. Hong, Z. Liu, X. Zhang, and S. Hark, "Self-catalytic growth of single-phase AlGaN alloy nanowires by chemical vapor deposition," *Applied physics letters,* vol. 89, no. 19, p. 193105, 2006.

[40] S. Wu *et al.*, "Influence of lateral growth on the optical properties of GaN nanowires grown by hydride vapor phase epitaxy," *Journal of Applied Physics,* vol. 122, no. 20, p. 205302, 2017.

[41] Y.-H. Ra, R. Navamathavan, J.-H. Park, and C.-R. Lee, "Coaxial In x Ga1–x N/GaN multiple quantum well nanowire arrays on Si (111) substrate for high-performance light-emitting diodes," *Nano Letters,* vol. 13, no. 8, pp. 3506-3516, 2013.

[42] M. Tchernycheva *et al.*, "InGaN/GaN core–shell single nanowire light emitting

diodes with graphene-based p-contact," *Nano Letters,* vol. 14, no. 5, pp. 2456-2465, 2014.

[43] W. Goh *et al.*, "Structural and optical properties of nanodots, nanowires, and multi-quantum wells of III-nitride grown by MOVPE nano-selective area growth," *Journal of Crystal Growth,* vol. 315, no. 1, pp. 160-163, 2011.

[44] Y. Wang *et al.*, "AlGaN nanowires grown on SiO2/Si (100) using graphene as a buffer layer," *Crystal Growth & Design,* vol. 19, no. 10, pp. 5516-5522, 2019.

[45] M. Belloeil, "Molecular beam epitaxy growth and optical characterization of GaN/AlGaN nanowire heterostructures emitting in the ultraviolet," Université Grenoble Alpes, 2017.

[46] A. Pierret *et al.*, "Growth, structural and optical properties of AlGaN nanowires in the whole composition range," *Nanotechnology,* vol. 24, no. 11, p. 115704, Mar 22 2013.

[47] B. J. May *et al.*, "Enhanced uniformity of III-nitride nanowire arrays on bulk metallic glass and nanocrystalline substrates," *Journal of Vacuum Science Technology B, Nanotechnology Microelectronics: Materials, Processing, Measurement, Phenomena,* vol. 37, no. 3, p. 031212, 2019.

[48] B. Le, X. Liu, N. Tran, S. Zhao, and Z. Mi, "An electrically injected AlGaN nanowire defect-free photonic crystal ultraviolet laser," *Optics Express,* vol. 27, no. 4, pp. 5843-5850, 2019.

[49] K. Choi, M. Arita, and Y. Arakawa, "Selective-area growth of thin GaN nanowires by MOCVD," *Journal of Crystal Growth,* vol. 357, pp. 58-61, 2012.

[50] W. Guo, M. Zhang, P. Bhattacharya, and J. Heo, "Auger recombination in III-nitride nanowires and its effect on nanowire light-emitting diode characteristics," *Nano Lett,* vol. 11, no. 4, pp. 1434-1438, 2011.

[51] T. Kohno *et al.*, "Internal quantum efficiency and nonradiative recombination rate in InGaN-based near-ultraviolet light-emitting diodes," *Japanese Journal of Applied Physics,* vol. 51, no. 7R, p. 072102, 2012.

[52] J. Lu, Y. Zhong, and S. Zhao, "Intrinsic excitation-dependent room-temperature internal quantum efficiency of AlGaN nanowires with varying Al contents," *Journal of Vacuum Science & Technology B,* vol. 39, no. 2, 2021.

[53] P. Zhu and N. Tansu, "Effect of packing density and packing geometry on light extraction of III-nitride light-emitting diodes with microsphere arrays," *Photonics Research,* vol. 3, no. 4, pp. 184-191, 2015.

[54] X.-H. Li *et al.*, "Light Extraction Efficiency Enhancement of III-Nitride Light-Emitting Diodes by Using 2-D Close-Packed TiO2 Microsphere Arrays," *Applied Physics Letters,* vol. 9, no. 5, pp. 324-332, 2013.

[55] P. Zhu, G. Liu, J. Zhang, and N. Tansu, "FDTD analysis on extraction efficiency of GaN light-emitting diodes with microsphere arrays," *Journal of Display Technology,* vol. 9, no. 5, pp. 317-323, 2013.

[56] Y.-K. Ee *et al.*, "Optimization of light extraction efficiency of III-nitride LEDs with self-assembled colloidal-based microlenses," *IEEE Journal of Selected Topics in Quantum Electronics,* vol. 15, no. 4, pp. 1218-1225, 2009.

[57] Y.-K. Ee, P. Kumnorkaew, H. Tong, R. A. Arif, J. F. Gilchrist, and N. Tansu, "Comparison of numerical modeling and experiments of InGaN quantum wells light-emitting diodes with SiO2/polystyrene microlens arrays," in *Light-Emitting Diodes: Research, Manufacturing, and Applications XII*, 2008, vol. 6910, p. 69100M: International Society for Optics and Photonics.

[58] Y. K. Ooi and J. Zhang, "Light extraction efficiency analysis of flip-chip ultraviolet light-emitting diodes with patterned sapphire substrate," *IEEE*

Photonics Journal, vol. 10, no. 4, pp. 1-13, 2018.

[59] S. Zhou *et al.*, "Comparative study of GaN-based ultraviolet LEDs grown on different-sized patterned sapphire substrates with sputtered AlN nucleation layer," *Japanese Journal of Applied Physics,* vol. 56, no. 11, p. 111001, 2017.

[60] X.-F. Li *et al.*, "Fabrication of patterned sapphire substrate and effect of light emission pattern on package efficiency," *Optical Materials Express,* vol. 5, no. 8, pp. 1784-1791, 2015.

[61] S. Hagedorn, A. Knauer, A. Mogilatenko, E. Richter, and M. Weyers, "AlN growth on nano-patterned sapphire: A route for cost efficient pseudo substrates for deep UV LEDs," *Physica Status Solidi,* vol. 213, no. 12, pp. 3178-3185, 2016.

[62] M. Kim *et al.*, "AlGaN-based deep ultraviolet light-emitting diodes fabricated on patterned sapphire substrates," *Applied Physics Express,* vol. 4, no. 9, p. 092102, 2011.

[63] H. Ichikawa and T. Baba, "Efficiency enhancement in a light-emitting diode with a two-dimensional surface grating photonic crystal," *Applied Physics Letters,* vol. 84, no. 4, pp. 457-459, 2004.

[64] A. A. Erchak *et al.*, "Enhanced coupling to vertical radiation using a two-dimensional photonic crystal in a semiconductor light-emitting diode," *Applied Physics Letters,* vol. 78, no. 5, pp. 563-565, 2001.

[65] S. Fan, P. R. Villeneuve, and J. D. Joannopoulos, "Rate-Equation Analysis of Output Efficiency and Modulation Rate of Photonic-Crystal Light-Emitting Diodes," *IEEE Journal of Quantum Electronics,* vol. 36, pp. 1123-1130, 2000.

[66] S. Fan, P. R. Villeneuve, and J. D. Joannopoulos, "High Extraction Efficiency of Spontaneous Emission from Slabs of Photonic Crystals," *Physical Review*

Letters, vol. 78, no. 17, p. 3295, 1997.

[67] I. Schnitzer, E. Yablonovitch, C. Caneau, T. J. Gmitter, and A. Scherer, "30% external quantum efficiency from surface textured, thin-film light-emitting diodes," *Applied Physics Letters,* vol. 63, no. 16, pp. 2174-2176, 1993.

[68] L. Dang Hoang, H. In-Kag, and R. Sang-Wan, "Design Optimization of Photonic Crystal Structure for Improved Light Extraction of GaN LED," *IEEE Journal of Selected Topics in Quantum Electronics,* vol. 15, no. 4, pp. 1257-1263, 2009.

[69] X. Liu, K. Mashooq, T. Szkopek, and Z. Mi, "Improving the Efficiency of Transverse Magnetic Polarized Emission from AlGaN Based LEDs by Using Nanowire Photonic Crystal," *IEEE Photonics Journal,* vol. 10, no. 4, pp. 1-11, 2018.

[70] B. Jain *et al.*, "Enhancing the light extraction efficiency of AlInN nanowire ultraviolet light-emitting diodes with photonic crystal structures," *Optics Express,* vol. 28, no. 15, pp. 22908-22918, 2020.

[71] Ž. Podlipskas *et al.*, "Dependence of radiative and nonradiative recombination on carrier density and Al content in thick AlGaN epilayers," *Journal of Physics D: Applied Physics,* vol. 49, no. 14, 2016.

[72] H. Murotani *et al.*, "Correlation between excitons recombination dynamics and internal quantum efficiency of AlGaN-based UV-A multiple quantum wells," *Journal of Applied Physics,* vol. 128, no. 10, p. 105704, 2020.